Journal Pre-proof

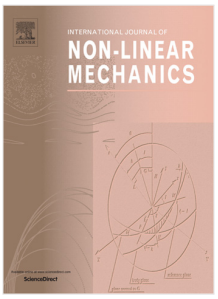

Dynamic buckling of classical/non-classical curved beams by nonlocal nonlinear finite element accounting for size dependent effect and using higher-order shear flexible model

De Sarthak, G. Prateek, R. Vasudevan, O. Polit, M. Ganapathi

PII: S0020-7462(20)30198-0
DOI: https://doi.org/10.1016/j.ijnonlinmec.2020.103536
Reference: NLM 103536

To appear in: *International Journal of Non-Linear Mechanics*

Received date : 20 May 2020
Revised date : 14 June 2020
Accepted date : 15 June 2020

Please cite this article as: D. Sarthak, G. Prateek, R. Vasudevan et al., Dynamic buckling of classical/non-classical curved beams by nonlocal nonlinear finite element accounting for size dependent effect and using higher-order shear flexible model, *International Journal of Non-Linear Mechanics* (2020), doi: https://doi.org/10.1016/j.ijnonlinmec.2020.103536.

Dynamic buckling of classical/non-classical curved beams by nonlocal nonlinear finite element accounting for size dependent effect and using higher-order shear flexible model

De Sarthak[a], G. Prateek[a], R. Vasudevan[a], O. Polit[b], M Ganapathi[a$]

[a]*School of Mechanical Engineering, Vellore Institute of Technology, Vellore, 632 014, India*
[b]*LEME, UPL, Univ. Paris Nanterre, 50 rue de Sevres, 92410, Ville d'Avray, France*

Abstract

This paper investigates the dynamic snap-through buckling of classical and non-classical curved beams subjected to a suddenly applied step load. The small scale effect prevalent in non-classical beams, *viz.*, micro and nanobeam, is modelled using the nonlocal elasticity approach. The formulation accounts for moderately large deflection and rotation. The governing equilibrium equations are derived using the dynamic version of the principle of virtual work and are subsequently simplified in terms of the generalized displacements for the development of a nonlocal nonlinear finite element model. The spatial domain comprises of 3-noded higher-order curved beam elements based on shear flexible theory associated with sine function. The nonlinear governing equations are solved using the incremental stiffness matrices and by adopting direct time integration method. The critical dynamic buckling load is identified by the smallest load at which there is a sudden rise in the amplitude of the vibration. The efficacy of model here is compared against the available analytical studies for the local and nonlocal beams. A detailed study is made to highlight the effects of the geometric parameter, initial condition, nonlocal parameter, load duration, and boundary conditions on the dynamic stability of both classical and non-classical curved beams. The nature and degree of participation of various eigen modes accountable for the dynamic snap-through behaviour are examined *a posteriori* using the modal expansion approach. Some interesting observations made here are valuable for the optimal design of such structural member against fatigue and instability.

Keywords: Nonlocal nonlinear analysis; Dynamic buckling; Classical curved beam; Curved nanobeam; Time response; Modal participation factor; Geometric parameter; snap-through

[$]Corresponding author

E-mail address: Ganapathi.M@vit.ac.in (M. Ganapathi).

Introduction

With slender structural elements subjected to increasingly complex and severe environments such as in shock loading on supersonic aircrafts, seismic loading on beams and wind gusts over roof etc., it becomes imperative to study the limits to their performance. Strength, resistance and other physical properties of structural elements are often estimated using data from static analysis and experiments; however structures can reach failure at loads much lower when subjected to dynamic loading. The problem of structures subjected to sudden loads for infinite duration has received significant attention in the study of dynamic stability. It is observed with only incremental changes in the load, the structure shifts from oscillating with sufficiently small amplitude about its static equilibrium to experiencing large-amplitude oscillations [1]. In the process the structure traverses an unstable static equilibrium configuration, emulating the static snap-through buckle. One of the first studies of the phenomenon was carried out by Budiansky and Roth [2] on spherical caps. Hoff and Bruce [3] analysed a simpler configuration, the half-sine arch under a similarly distributed load. In the present work an extensive study of the dynamic stability of classical/non-classical curved beam is carried out. Due to its simplicity, it has received exhaustive attention in literature and thus a brief discussion of the existing work is provided here to bring out the widely used methods, the limitation of the solution approaches, and the accepted results, etc.

Huang *et al.* [4] studied the dynamic snap-buckling of hinged sinusoidal arches under the influence of a sudden load for infinite duration. The governing equations were derived using the principle of force and momentum balance wherein the geometric nonlinearity was incorporated via the component of horizontal thrust. The system was simplified into two equations by assuming only the first (symmetric) and second harmonic (asymmetric) modes as the solution. The critical loads were identified using both the saddle point on the potential surface and the criterion outlined in the work of Budiansky and Roth [2]. A decrease in the critical load was noted in the presence of an initial asymmetric imperfection. A rigorous analytical approach was carried out in Ref. [5] where the problem setup was similar to that of given in Ref. [4]. It brought out the effects of damping on the system, it was found that, beyond a certain arch rise, the critical loads calculated from static analysis and a damped dynamical system were same. Critical cases were identified using the criterion of dynamic stability in the sense of Liapunov. *Hsu et al.* [6] provided an extensive analysis of the dynamic instability of clamped shallow arches, by studying simple, normal and parabolic arches under different configuration of loads. Here, instead of assuming a Fourier series solution, the

normalized buckling eigen modes of a simple column clamped at both ends were used, ensuring that the modes were decoupled statically. Humphreys [7] adopted a more universal definition for the arch, and reported a net decrease in the critical load with the increase in the non-dimensional geometry parameter and the magnitude of initial imperfection. A limited sine series solution was used to solve the governing equation. With various different boundary conditions, initial conditions, loadings, and solution methodologies such as Galerkin approach, direct substitution, etc., the problem of dynamic buckling has been solved majorly, using an *a priori* assumption on the solutions based on the flat column in the literature [8-12].

Sheinman [13] employed an interlaced finite difference grid, which resembles elements used in finite element analysis to avoid shear locking, with in-plane displacements on one grid, and out of plan on the adjacent alternate points. It was found that increasing the shear stiffness of the beams resulted in higher frequencies; however the critical buckling loads remained the same. Chien and Palazotto [14] focussed on the dynamic buckling of composite cylindrical panels using an isoparametric shell element and incorporated higher-order transverse shear deformation. The various examples were explained using phase plane diagrams to highlight the chaotic nature of the dynamic snap-through buckling. The *beta-m* time integration scheme was used to register the dynamic response, and inflection points in the response were used to identify the critical loads. Pi and Bradford [15] studied the dynamic buckling phenomenon over the shallow circular arches under a sudden uniform circular load using the finite element method wherein the results confirmed that the dynamic critical loads were lower than the static buckling loads for various boundary conditions. Yang *et al.* [16] studied the dynamic buckling of functionally graded graphene platelets (FG-GPLs) reinforced composite shallow arches under a concentrated step load by using an analytical approach to compute the nonlinear equilibrium path and identifying the limit point for dynamic buckling load; the results were shown to have good agreement with a ANSYS based FE model. Chandra *et al.* [17] employed the finite element approach in conjunction with the experimental analysis for characterizing the dynamic transitions associated with the snap through of shallow arches. The nonlinear thermal-dynamic buckling of curved beams was studied in [18] using the finite element approach, where the importance of an elastic foundation was highlighted in making the post-equilibrium unstable for the occurrence of dynamic buckling. Other studies employing mesh based methods to study dynamic buckling are reported in Refs. [19-23]. Most mesh and FEM based investigations employed models based on the classical or first-shear deformation theory, they provided a

limited parametric study related to initial conditions, geometry parameter and rarely brought out discussion on the participating modes in the registered response.

To address the need for making devices which consume lesser space and are equally resilient, sectors ranging from aerospace, energy to medicine have shown a growing interest in the broad discipline of nanotechnology. Complex systems and devices make use of structural elements ranging in size from 1-100*nm*. This has necessitated the study of their behaviour in response to various types of loadings. Important studies employing the use of a non-local elasticity approach to incorporate the small-scale effects prominent in nanobeam are listed in [24-28]. While the aforementioned studies are linear in nature, Ghayesh *et al.* introduced non-linear terms to incorporate the membrane stretching effect coupled with different theories to model the size-dependent effect in [29,30] to analyse the nonlinear dynamics of a straight microbeam using the Galerkin's approach. The modelling and simulation on the behaviour of straight macro/nanobeams is exhaustive; literature exploring the instabilities curved micro/nanostructures is rather meagre. While in the macro regime, failure due to dynamic buckling renders the structure useless; in micro/nanostructures it finds application in radio-frequency (RF) switches, accelerometers, pressure sensors and bio-MEMS. Das and Batra [31,32] carried out extensive analysis of the dynamic instabilities *i.e.* snap-through and pull-in instability in microelectromechanical shallow arches. The nonlinear contribution to the governing equation was introduced from the stretching and voltage terms making it susceptible to dynamic instability. A series like function of the eigen modes of an undamped straight beam was assumed to solve the nonlinear partial differential equations. Ref. [33] presented solutions to the problem of bifurcation buckling of nanorings and arches for the static case; a relation for the case of buckling using a Fourier series assumption for the displacement was derived. The size dependent effects were modelled using the Eringen's nonlocal theory. The study reported a reduction in critical load with the increase in nonlocal parameter. The study by Kaviani and Mirdamadi [34] analysed static snap-through and bifurcation of nano-arches on a Winkler elastic foundation, using both the strain gradient and Eringen's nonlocal theory. The foundation modulus was found to increase the stability of the system and in some cases change the type of mechanism for instability. She *et al.* [35] investigated the snap-through buckling in functionally graded porous curved nanobeams using the two step perturbation technique. While the work on nonlinear static buckling of the non-classical curved beam is very much limited, studies dealing with

the nonlinear transient analysis and dynamic stability of such class of beam are not yet commonly available in the literature.

The review of literature made here suggests that a systematic approach through nonlinear dynamic response analysis in conjunction with higher-order shear deformation theory without imposing any restriction on the mode shapes for analysing the snap-buckling of arch or curved beam, in general, is warranted to predict the behavioural trends of classical and non-classical curved structures more accurately allowing one to establish general principles for designing complex nanodevices. The present study, in order to fill the gap in the literature, thus focuses on deriving the governing equilibrium equations through Hamilton's principle in terms of generalized displacements for the development of nonlocal nonlinear dynamic finite element formulation for curved beam. The geometric nonlinearity, based on the Lagrangian strain components, is approximated to account for the moderate large displacement and rotation. The size dependent effect associated with non-classical beam, viz., micro and nanobeam, is introduced through nonlocal elasticity theory [36, 37]. A higher-order shear flexible finite element employing the trigonometric shear deformation theory described in Touratier [38] and Polit and Touratier [39] is integrated with the finite element model. The incremental stiffness matrices evolved from nonlinear finite element procedure are reformulated to result in symmetric matrices as this improves the computational efficiency. The resulting nonlinear equations are then solved using the Newmark's time integration procedure coupled with the Newton-Raphson iterative scheme in establishing the equilibrium position at every time step. The dynamic snap-through of classical and non-classical curved beams is identified by examining the load-deflection relationship evolved through the time responses obtained for various loads. An extensive modal expansion study is subsequently conducted to extract the participation of various natural vibration modes dictating for the change in the buckling trend of classical/non-classical curved beams. The work presents a rigorous and quantitative analysis of the critical loads with respect to the geometric parameter, nonlocal parameter, boundary conditions, initial conditions, applied load duration, and also mode participation in the snap–through.

The paper is structured as: Curved beam classical continuum model is dealt in Section 2, followed by Non-classical or local formulation in Section 3; governing equations through matrix formulation is outlined in Section 4 and finite element methodology and solution approach are presented in Section 5; results and discussion are shown in Section 6, followed by the conclusion based on the detailed study.

2. Classical curved beam model

In the present work, a curved beam of length L, with a rectangular cross section S and an associated local curvilinear system is considered, Fig. 1a. Curvilinear coordinate $x \in [0, L]$ is taken along the arc length of the curved beam whereas $z \in [-h/2, h/2]$ is assumed along the thickness of the beam. The y coordinate is associated with the width of the beam and is not considered in the formulation. R is the constant radius of curvature of the beam. Here, a wide range of beams can be studied by varying the thickness h and the open angle ϕ of the curved beam.

2.1 Constitutive relation

Considering a two-dimensional model of an isotropic curved beam, the constitutive equations are given as

$$\begin{cases} \sigma_{xx} = C_{11}\varepsilon_{xx} \\ \sigma_{xz} = C_{66}\gamma_{xz} \end{cases} \quad (1)$$

where the stiffness coefficients C_{11} & C_{66} are equal to Young's modulus, E and shear modulus, G, respectively.

2.2 Displacement field

The present formulation incorporates the shear deformation theory based on sine function, denoted as SIN [38, 39], and developed for various applications on beams, plates and shells. The displacement kinematics of the proposed model are represented by

$$\begin{cases} u(x,z) = \left(1 + \frac{z}{R}\right) u_0(x) - z{w'}_0(x) + f(z)\,\gamma_0(x) \\ w(x,z) = w_0(x) \end{cases} \quad (2a)$$

where the function γ_0 is the defined as

$$\gamma_0(x) = \theta(x) + {w'}_0(x) - \frac{1}{R}u_0(x) \quad (2b)$$

This SIN model makes use of three field variables i.e. u_0 (x, t) referring the curvilinear axial displacement; w_0 (x, t) as the transverse displacement of mid-line point of the beam; $\theta(x, t)$ associating with rotation of the section. Lastly,

t is the temporal variable. In the current work, the spatial and temporal derivatives are denoted as $(\,)' = \frac{d}{dx}$ and $\dot{(\,)} = \frac{d}{dt}$, respectively.

In Eq. (2a), the definition of the function $f(z)$ allows us to compute the bending deformation of beam for different theories available in literature, as seen in Fig. 2 such as Euler-Bernoulli by letting $f(z) = 0$; Timoshenko by $f(z) = z$; SIN model by $f(z) = \frac{h}{\pi}\sin\frac{\pi z}{h}$.

2.3 Strain Field

The strain components are evolved classically with respect to the curvilinear covariant basis vector and we recover the following relations, omitting the coordinates (x, t) & (z) from the displacement functions for simplicity and introducing derivative $(\,)_{,z} = \frac{d}{dz}$ as

$$\varepsilon_{xx} = \left(1+\frac{z}{R}\right)^{-1}\left(u' + \frac{1}{R}w\right)$$

$$\gamma_{xz} = u_{,z} + \left(1+\frac{z}{R}\right)^{-1}\left(w' - \frac{1}{R}u\right) \tag{3}$$

From the kinematics defined in Eq. (2a), introducing some simplifications & assumptions, $\frac{1}{(1+z/R)} \approx 1$ and neglecting higher order terms, the linear strain components from Eq. (3) can be shown in terms of displacement variables as

$$\varepsilon_{xx}^{L} = u_0' + \frac{1}{R}w_0 + z\left(\frac{1}{R}u_0' - w_0''\right) + f\gamma_0' \tag{4a}$$

$$\gamma_{xz}^{L} = f_{,z}\gamma_0$$

Using the appropriate simplification to the Lagrangian strain components and retaining for the moderate large deflection and rotation effects, the total strain components can be written as [40]

$$\varepsilon_{xx} = \varepsilon_{xx}^{L} + \frac{1}{2}(w_0')^2 + \frac{1}{2}f^2(\theta')^2 + f\theta' u_0'$$

$$\gamma_{xz} = \gamma_{xz}^{L} + f f_{,z}\,\theta\theta' + f_{,z}\theta u_0' \tag{4b}$$

2.4 Stress, force and moment field for local analysis

For the classical elasticity analysis, the stress field is directly deduced from the constitutive relation given in Eq. (1) and the strain components in Eq. (4). On the other hand, the force and moment fields are defined from the stress components as follows:

$$\left[N_{xx}, M_{xx}, \widehat{M}_{xx}, M^{*}_{xx}\right] = \int_{-h/2}^{h/2} [1, z, f, f^2]\, \sigma_{xx}\, dz$$

$$\left[\hat{Q}_{xz}, Q^{*}_{xz}\right] = \int_{-h/2}^{h/2} [\, f_{,z},\ f f_{,z}]\sigma_{xz}\, dz \qquad (5)$$

2.5 Variational statements

The governing equations of motion in terms of displacements are derived using Hamilton's Principle. The dynamic version of the principle of virtual work takes the following form

$$0 = \int_0^T (\delta U + \delta V - \delta K)\, dt \qquad (6)$$

where δU & δK are the variation of the strain energy and kinetic energy, respectively; δV is variation of the work done by the applied load.

Taking into account the force and moment fields Eq. (5), the variation of the strain energy is written in terms of the force and moment fields and the variation of the displacements given in Eq. (2) as

$$\delta U_e = \int_0^L \int_{-h/2}^{h/2} (\delta\, \varepsilon_{xx}^{T}\, \sigma_{xx})\, dz dx + \int_0^L \int_{-h/2}^{h/2} (\delta\, \gamma_{xz}^{T}\, \tau_{xz})\, dz dx =$$

$$\int_0^L \begin{bmatrix} N_{xx}\left(\delta u'_0 + \frac{1}{R}\delta w_0 + w'_0 \delta w'_0\right) + M_{xx}\left(\frac{1}{R}\delta u'_0 - \delta w''_0\right) + M^{*}_{xx}\theta'\delta\theta' + \widehat{M}_{xx}(\theta'\delta u'_0 + u'_0\delta\theta') \\ +\widehat{M}_{xx}\delta\gamma'_0 \\ +\hat{Q}_{xz}\delta\gamma_0 + Q^{*}_{xz}(\theta\delta\theta' + \theta'\delta\theta) + \hat{Q}_{xz}(u'_0\delta\theta + \theta\delta u'_0) \end{bmatrix} dx \qquad (7)$$

Following the same approach for the variation of the kinetic energy, we obtain as

$$\delta K = \int_0^L \left(\left(-I_1\ddot{u}_0 - I_2\ddot{w}'_0 - I_3\ddot{\theta}\right)\delta u_0 + \left(I_2\ddot{u}'_0 + I_4\ddot{w}''_0 + I_5\ddot{\theta}' - I_0\ddot{w}_0\right)\delta w_0 + \left(-I_3\ddot{u}_0 - I_5\ddot{w}'_0 - I_6\ddot{\theta}\right)\delta\theta\right) dx \qquad (8a)$$

where, $[I_0, I_1, I_2, I_3] = \rho \int_{-h/2}^{h/2} [1, A^2, A\,(f - z), A\, f]\, dz$; $A = \left(1 + \frac{z}{R} - \frac{f}{R}\right)$

$$[I_4, I_5, I_6] = \rho \int_{-h/2}^{h/2} [(f - z)^2, (f - z)f, f^2]\, dz \qquad (8b)$$

Here, the curved beam is subjected to externally applied distributed force $p(x, t)$ acting on the upper surface ($z = h/2$). The variation of work done by the applied force, as part of the potential energy contribution, can be written as

$$\delta V = -\int_0^L p\ \delta w_0\ dx \tag{9}$$

2.6 Equations of motion

The governing equations are derived from the variational principle Eq. (6), introducing Eqs. (7)-(9), proceeding some integrations by parts and they are presented here as

$$\delta u_0: -N'_{xx} - \frac{1}{R}\left(M'_{xx} - \widehat{M}'_{xx}\right) - \frac{1}{R}\hat{Q}_{xz} - \left(\widehat{M}'_{xx}\theta' + \widehat{M}_{xx}\theta''\right) - \left(\hat{Q}'_{xz}\theta + \hat{Q}_{xz}\theta\right) = \left(-I_1\ddot{u}_0 - I_2\ddot{w}'_0 - I_3\ddot{\theta}\right)$$

$$\delta w_0: \frac{1}{R}N_{xx} - \left(M''_{xx} - \widehat{M}''_{xx}\right) - \hat{Q}'_{xz} - N_{xx}w''_o - N'_{xx}w'_o - q = \left(I_2\ddot{u}'_0 + I_4\ddot{w}_0{}'' + I_5\ddot{\theta}' - I_0\ddot{w}_0\right)$$

$$\delta\theta: -\widehat{M}'_{xx} + \hat{Q}_{xz} - \left(M^*_{xx}{}'\theta' + M^*_{xx}\theta''\right) - Q^*_{xz}{}'\theta - \left(\widehat{M}'_{xx}u'_0 + \widehat{M}_{xx}u''_0\right) + \hat{Q}_{xz}u'_0 = \left(-I_3\ddot{u}_0 - I_5\ddot{w}'_0 - I_6\ddot{\theta}\right) \tag{10}$$

Eq. (10), in general, can be used for solving any class of problems as it is derived in terms of stress and moment resultants. The essential and natural boundary conditions associated with the present theory are as follows:

$$u_0 \text{ or } \left[N_{xx} + \frac{(M_{xx} - \widehat{M}_{xx})}{R} + \widehat{M}_{xx}\theta' + \hat{Q}_{xz}\theta\right]$$

$$w_0 \text{ or } \left[\hat{Q}_{xz} + M'_{xx} - \widehat{M}'_{xx} + N_{xx}w'_o + I_2\ddot{u}'_0 + I_4\ddot{w}''_0 + I_5\ddot{\theta}'\right] \tag{11}$$

$$\theta \text{ or } \left[\widehat{M}_{xx} + M^*_{xx}\theta' + Q^*_{xz}\theta + \widehat{M}_{xx}u'_0\right]$$

The governing equation of motion Eq. (10) is either analytically or numerically solved.

3. Non-classical (nonlocal) formulation

The most accurate methods in modeling nanostructures are atomistic approaches such as molecular dynamics, density functional theory etc., however they are computationally very expensive making in-depth analysis of dynamical systems unfeasible. Continuum mechanics based approaches are simpler and make studying the various structural behaviors of nanostructures easier. While the classical elasticity theories are size free and can be applied to a wide range of length and time scale of structures, their accuracy in predicting behavior greatly depends on the relation between the internal characteristic length and the external parameter. The nonlocal theories are based on size dependent continuum mechanics that model the small scale effects in the constitutive equations.

These theories are derived using laws such as the energy balance law being valid globally, the constitution-dependent variables and also stress-driven formulation of nonlocal elasticity. One of the major ways the non-local model differs from the classical approach is that stress at a point in a continuum body depends not only on the strain at that point but also on strains at all points of the body.

3.1 Nonlocal constitutive relations

The nonlocal constitutive behaviour of a Hookean solid is represented in the differential form as proposed by Eringen [36, 41] and extended for the beam in [37, 42] as:

$$(1 - l^2\tau^2\nabla^2)\sigma_{ij} = \sigma_{ij}^L \qquad (12)$$

Here, σ_{ij} & σ_{ij}^L are the nonlocal and local stress tensors. The local stress tensor σ_{ij}^L at a point can be related to strain tensor by the generalized Hooke's law. τ^2 is equal to μ/l^2; where μ is defined as the nonlocal parameter and is a dimensional quantity, $(nm)^2$ equal to $(e_0a_0)^2$; e_0 is a constant appropriate to each material, a_0 is an internal characteristic length (e.g. length of CC bond, lattice parameter, granular distance), l is an external characteristic length (e.g. crack length, wavelength). The value of e_0 is determined from experiments or by matching dispersion curves of plane waves with those of atomic lattice dynamics. An estimation of the value was proposed by Wang [43] in CNT beam like wave motion studies. μ is also referred to as the scale coefficient revealing the small scale effect on the response of structures of nano-size. A conservative estimate of (e_0a_0) < 2 nm is taken for SWCNT if the measured wave propagation frequency value for SWCNT is greater than 10 THz. It is further seen from literature that the value of μ is considered in the range of 0–4$(nm)^2$ for most of the theoretical studies based on nonlocal analysis. The Laplacian in Eq. (12) can be replaced using a double derivative in a one dimensional model for the various stress components involved in the present curved beam theory considered here as:

$$\sigma_{xx} - \mu\,\sigma_{xx}'' = \sigma_{xx}^l$$

$$\sigma_{xz} - \mu\,\sigma_{xz}'' = \sigma_{xz}^l \qquad (13a)$$

Eq. (13a) can be rewritten by expressing the local stress components σ_{ij}^L using the constitutive relation given in Eq. (1) as:

$$\sigma_{xx} - \mu\,\sigma_{xx}'' = C_{11}\varepsilon_{xx}$$

$$\sigma_{xz} - \mu\,\sigma_{xz}'' = C_{66}\gamma_{xz} \tag{13b}$$

By integrating Eq. (13a) over cross-sectional area of the beam, the relations between the stress/moment resultants involved in the present local theory and nonlocal theory are defined as:

$$\left[(N_{xx} - \mu\,N_{xx}''), (M_{xx} - \mu\,M_{xx}''), \left(\widehat{M}_{xx} - \mu\,\widehat{M}_{xx}''\right), (M_{xx}^* - \mu\,M_{xx}^*'')\right] = \left[N_{xx}^l, M_{xx}^l,\ \widehat{M}_{xx}^l, M_{xx}^{*l}\right]$$

$$\left[\left(\hat{Q}_{xz} - \mu\,\hat{Q}_{xz}''\right), (Q_{xz}^* - \mu\,Q_{xz}^*'')\ \right] = \left[\ \hat{Q}_{xz}^l,\ \ Q_{xz}^{*l}\right] \tag{14}$$

Here, the stress/moment resultants in local shear deformation theory considered here $\left[N_{xx}^l, M_{xx}^l, \widehat{M}_{xx}^l, M_{xx}^{*l}\right]$ can be defined in terms of strains by introducing Eq. (4) in Eq. (5) as:

$$\left[N_{xx,}^l\, M_{xx,}^l\ \widehat{M}_{xx,}^l M_{xx}^{*l}\right] = \int_{-h/2}^{h/2}[1, z, f, f^2]\ C_{11}\varepsilon_{xx}\,dz$$

$$\left[\ \hat{Q}_{xz}^l, Q_{xz}^{*l}\right] = \int_{-h/2}^{h/2}\left[f_{,z}, ff_{,z}\right]\ C_{66}\gamma_{xz}\,dz \tag{15}$$

3.2 Nonlocal equilibrium equations

Substituting the expressions obtained for stress and moment resultants $\left[N_{xx}, M_{xx}, \widehat{M}_{xx}, M_{xx}^*\right]$ & $\left[\hat{Q}_{xz}, Q_{xz}^*\right]$ for nonlocal theory from Eq. (14) into Eq. (10) and then simplifying the resulting equations, we obtain the following governing equations in terms of local stress resultants as

$$\delta u_0: -N_{xx}^{l\,\prime} - \frac{1}{R}\left(M_{xx}^{l\,\prime} - \widehat{M}_{xx}^{l\,\prime}\right) - \frac{1}{R}\hat{Q}_{xz}^l - \left(\widehat{M}_{xx}^{l\prime}\theta' + \widehat{M}^{l}{}_{xx}\theta''\right) - \left(\hat{Q}_{xz}^{l\prime}\theta + \hat{Q}^{l}{}_{xz}\theta\right) =$$

$$\left(1 - \mu\,\frac{d^2}{dx^2}\right)\left(-I_1\ddot{u}_0 - I_2\ddot{w}_0' - I_3\ddot{\theta}\right)$$

$$\delta w_0: \frac{1}{R}N_{xx}^l - \left(M_{xx}^{l\,\prime\prime} - \widehat{M}_{xx}^{l\,\prime\prime}\right) - \hat{Q}_{xz}^{l\,\prime} - N_{xx}^l w_o'' - N_{xx}^{l\,\prime} w_o' =$$

$$\left(1 - \mu\,\frac{d^2}{dx^2}\right)\left(q + \left(I_2\ddot{u}_0' + I_4\ddot{w}_0'' + I_5\ddot{\theta}' - I_0\ddot{w}_0\right)\ \right)$$

$$\delta\theta: -\widehat{M}_{xx}^{l\,\prime} + \hat{Q}_{xz}^l - \left(M_{xx}^{*l\,\prime}\theta' + M_{xx}^{*l}\theta''\right) - Q_{xz}^{*l\,\prime}\theta - \left(\widehat{M}_{xx}^{l\prime}u_0' + \widehat{M}^{l}{}_{xx}u_0''\right) + \hat{Q}^{l}{}_{xz}u_0' =$$

$$\left(1 - \mu\,\frac{d^2}{dx^2}\right)\left(-I_3\ddot{u}_0 - I_5\ddot{w}_0' - I_6\ddot{\theta}\right) \tag{16}$$

A weak formulation can be obtained from Eqs. (7)–(9) and introducing nonlocal equilibrium equation Eq. (16). One can also apply the principle of virtual displacement to derive the variational statements as outlined in *Appendix* A.

4. Matrix formulation of the nonlocal variational statements

The governing equation for dynamic analysis can be obtained from the variational statements derived in Appendix A. For a curved non-classical beam (nanobeam) subjected to transverse load *p* acting on the upper surface ($z = h/2$), the weak form incorporating small scale effects is expressed as follows:

$$\int_0^L \int_{-h/2}^{h/2} (\delta\varepsilon_{xx}^T C_{11}\varepsilon_{xx}) dz dx + \int_0^L \int_{-h/2}^{h/2} (\delta\gamma_{xz}^T C_{66}\gamma_{xz})\, dz dx = \int_0^L \left[\delta\{\bar{u}\}^T \left(1 - \mu \frac{d^2}{dx^2}\right)\{r\} + \int_{-h/2}^{h/2} \delta\{\bar{u}\}^T \left(1 - \mu \frac{d^2}{dx^2}\right)\rho\{\ddot{\bar{u}}\}\, dz\right] dx \quad (17a)$$

where $\{\bar{u}\}$ is the vector containing the displacements (u, w) from Eq. (2), is rewritten as

$$\{\bar{u}\} = [F_{uw}(z)]\{\varepsilon_{uw}\} \quad (17b)$$

$$\text{Here, } [F_{uw}(z)] = \begin{bmatrix} 1 & z & f & 0 \\ 0 & 0 & 0 & 1 \end{bmatrix}; \{\varepsilon_{uw}\}^T = \begin{bmatrix} u_0 & \left(\frac{u_0}{R} - w_0'\right) & \gamma_0 & w_0 \end{bmatrix}; \{r\}^T = [0 \quad p] \quad (17c)$$

Following the procedure outlined by Ganapathi and Varadan [44], the variation of strain energy functional given in LHS of Eq. (17a) can be expressed in terms of incremental stiffness matrices that are reformulated into symmetric forms as

$$\int_0^L \{\delta d\}^T \left[[\hat{K}] + \left(\frac{1}{2}\right)[\hat{N}_1] + \left(\frac{1}{3}\right)[\hat{N}_2] + [\hat{N}_3]\right]\{d\}\, dx = \int_0^L \delta\{\varepsilon_{uw}\}^T\{R\} dx - \int_0^L \delta\{\varepsilon''_{uw}\}^T \mu\{R\} dx + \int_0^L \delta\{\varepsilon_{uw}\}^T[\hat{M}]\{\ddot{\varepsilon}_{uw}\}\, dx + \int_0^L \delta\{\varepsilon'_{uw}\}^T \mu\, [\hat{M}]\{\ddot{\varepsilon}'_{uw}\}\, dx \quad (18a)$$

$$\text{where } [\hat{M}] = \int_{-h/2}^{h/2} [F_{uw}(z)]^T \rho\, [F_{uw}(z)] dz\, ; \{R\} = \int_{-h/2}^{h/2} [F_{uw}(z)]^T \{r\}\, dz. \quad (18b)$$

The vectors $\{d\}^T$involving derivatives of fields variables with respective to the strain components ε_{xx} & γ_{xz} are defined as

$$\{\mathrm{d}\}^T = \left[\left(u_0' + \frac{w_0}{R}\right) \quad \left(\frac{u_0'}{\mathrm{R}} - w_0''\right) \quad \left(w_0'' + \theta' - \frac{u_0'}{\mathrm{R}}\right) \quad \gamma_0 \quad w_0' \quad \theta \quad \theta' \quad u'_0\right] \quad (19)$$

The development of various matrices $[\hat{M}], [\hat{K}], [\hat{N}_1], [\hat{N}_2]$ & $[\hat{N}_3]$ in Eq. (18a) is given in *Appendix* B.

5. Finite element approximations

5.1 Approximation for geometry

To develop the finite element model, the curved beam is first discretized into a set of elements of length l_e for a generic finite element Ω_e. The beam element given in Fig. 1b is defined by three nodes along the element local *x*-axis. The nodal coordinates x is approximated on the reference length with respect to the reduced coordinates ξ by:

$$x(\xi) = \frac{1+\xi}{2} l_e \tag{21}$$

5.2 Approximations for displacement

The generalized displacements are given in Eq. (2) have to be approximated by FEM. Therefore, the following functions have to be approximated:

• displacements of a mid-line point of the beam (u_0, w_0)

• rotation (θ)

Using standard quadratic shape functions, the curvilinear axial displacement $u_0(\xi)$ and the rotation $\theta(\xi)$ are defined as:

$$\{u_0\} = [N_u]\{q_{u_0}\}; \qquad \{\theta\} = [N_u]\{q_\theta\} \tag{22a}$$

$$\text{where, } [N_u] = \left[\frac{\xi(\xi-1)}{2} \quad \frac{\xi(\xi+1)}{2} \quad 1-\xi^2\right] \tag{22b}$$

with $[N_u]$, the quadratic shape functions and $\{q_{v_0}\}$ and $\{q_\theta\}$, the nodal degrees of freedom vectors on each element.

In the present work, the cubic function in the form of Hermite interpolation is employed for the transverse displacement in order to use a conforming finite element approximation technique and to avoid membrane and shear locking phenomena. This is ensured by recruiting $\{w_0, w_0'\}$ as the nodal degrees of freedom. The transverse displacement w_0 can be expressed in terms of nodal degrees of freedom as:

$$\{w_0\} = [N_w]\left[q_{w_0}\right] \tag{23a}$$

$[N_w]$is the Hermite interpolation functions, $\{q_{w_0}\}$ denotes the degrees of freedom for the unknown function w_0

Here:

$$[N_w] = \left[\frac{1}{4}(\xi^3 - 3\xi + 2) \quad \frac{l_e}{8}(\xi^3 - \xi^2 - \xi + 1) \quad \frac{1}{4}(\xi^3 + 3\xi + 2) \quad \frac{l_e}{8}(\xi^3 + \xi^2 - \xi - 1)\right] \tag{23b}$$

$$\{q_{w_0}\}^T = \left[w_0^{(1)} \;\; w'^{(1)}_0 \;\; w_0^{(2)} \;\; w'^{(2)}_0\right] \tag{23c}$$

The superscripts (1) and (2) the first and the last end nodes of the element ($\xi = \pm 1$), see Fig. 1b.

Let us consider the following vector $\{q_e\}$ of total nodal degrees of freedom for a generic elementary domain Ω_e:

$$\{q_e\}^T = \left[u_0^{(1)} \;\; w_0^{(1)} \;\; w'^{(1)}_0 \;\; \theta^{(1)} \;\; u_0^{(3)} \;\; \theta^{(3)} \;\; u_0^{(2)} \;\; w_0^{(2)} \;\; w'^{(2)}_0 \;\; \theta^{(2)}\right] \tag{24}$$

From Eq. (17c) and Eq. (19), the vectors $\{\varepsilon_{uw}\}$ and $\{d\}$ are expressed in terms of the elemental degrees of freedom vector $\{q_e\}$ using Eqs. (22) and (23):

$$\{\varepsilon_{uw}\} = [B_{uw}]\{q_e\}\,; \qquad \{\varepsilon'_{uw}\} = [B'_{uw}]\{q_e\}\,; \qquad \{\varepsilon''_{uw}\} = [B''_{uw}]\{q_e\}$$

$$\{d\} = [B_\varepsilon]\{q_e\}$$

$$\{w''_0\} = [N''_w]^T\{q_{w_0}\} \tag{25}$$

where $[B_{uw}]$ and $[B_\varepsilon]$ are matrices with sizes 4×10 and 8×10, respectively, collecting the shape function N_u, N_w and their derivatives terms. Substituting Eq. (25) in Eq. (18), the global equilibrium equation for the nonlinear dynamic problem is rewritten as:

$$[M]\{\ddot{q}\} + \left[[K] + \frac{1}{2}[N_1(q)] + \frac{1}{3}[N_2(q)] + [N_3]\right]\{q\} = \{F\} \tag{26}$$

Here, $\{q\}$ is the global degrees of freedom vector of the beam. $[M]$ is the consistent mass matrix; $[K]$ is the linear stiffness matrix due to membrane & bending; $[N_1]$ & $[N_2]$ are the nonlinear incremental stiffness matrices dependent linearly and quadratically on the physical field variables, respectively; $[N_3]$ corresponds to transverse shear stiffness matrix; $\{F\}$ represents the external force vector. They are obtained by assembling the individual element contributions, with superscript *e*, using the elementary matrices given as:

$$[K^e] = \int_0^l [B_\varepsilon]^T \left[\hat{K}\right][B_\varepsilon]\, dx \tag{27a}$$

$$[N_1^e] = \int_0^l [B_\varepsilon]^T \left[\hat{N}_1\right][B_\varepsilon]\,dx;\ [N_2^e] = \int_0^l [B_\varepsilon]^T \left[\hat{N}_2\right][B_\varepsilon]\,dx;\ [N_3^e] = \int_0^l [B_\varepsilon]^T \left[\hat{N}_3\right][B_\varepsilon]\,dx \quad (27b)$$

$$[M^e] = \int_0^l [B_{uw}]^T [m_{\varepsilon\varepsilon}][B_{uw}]\,dx + \mu \int_0^l [B'_{uw}]^T [m_{\varepsilon\varepsilon}][B'_{uw}]dx \quad (27c)$$

$$\{F\} = \int_0^l [B_{uw}]^T \{R\}\,dx - \mu \int_0^l [B''_{uw}\{R\}]^T dx \quad (27d)$$

A Gaussian numerical integration over the length and the thickness is used to evaluate the different elementary matrices.

The element proposed here uses the field consistency principle [45, 46] to make the model free from locking problems. By defining the shape functions of different orders of polynomials for u_0, w_0, & θ, the transverse shear strain $(\theta + w'_0 - \frac{1}{R}u_0)$ for γ_{xz}, Eq. (4a) is developed in a consistent way for avoiding the spurious shear energy issue. However, the shape functions used for v_0, w_0 in evaluating the membrane strain $(u'_0 + \frac{w_0}{R})$ represented by the first two terms in the expression for ε_{xx}, Eq. (4a) does not satisfy the consistency principle [45, 46], leading to locking in membrane energy for very thin beam. By finding the substitute shape function for w_0 to be consistent with u_0 [45, 46], the membrane locking problem is resolved.

5.3 Solution methodology

For the transient response, the implicit direct time-integration method proposed in [47] is used to solve Eq. (26) in the global sense and its details are given here. With prior knowledge of the solution at time t, this method provides a mean to determine the displacements at time $t + \Delta t$ by considering the equilibrium equations at time $t + \Delta t$ as

$$[M]\{\ddot{q}\}_{t+\Delta t} + \left[[N(q)]\{q\}\right]_{t+\Delta t} = \{F\}_{t+\Delta t} \quad (28)$$

where $\{\ddot{q}\}_{t+\Delta t}$ and $\{q\}_{t+\Delta t}$ are the nodal acceleration and displacement vectors, respectively at time $t + \Delta t$. $[[N(q)]\{q\}]_{t+\Delta t}$ is the internal force vector at time $t + \Delta t$ which can be expressed as

$$\left[[N(q)]\{q\}\right]_{t+\Delta t} = \left(\left[[K] + (1/2)[N_1(q)] + (1/3)[N_2(q)] + [N_3]\right]\{q\}\right)_{t+\Delta t} \quad (29)$$

In establishing the above equations, the tangent stiffness approach is utilized to express the internal forces $\left[[N(q)]\{q\}\right]$ at time $t + \Delta t$ as a function of the internal forces at time t as

$$\left[[N(q)]\{q\}\right]_{t+\Delta t} = \left[[N(q)]\{q\}\right]_t + [K_T(q)]_t\{\Delta q\} \quad (30)$$

where $[K_T(q)]_t = \left[[K] + [N_1] + [N_2] + [N_3]\right]$ is the tangent stiffness matrix and $\{\Delta q\} = \{q\}_{t+\Delta t} - \{q\}_t$.

Substituting Equation (30) into Eq. (28), the governing equation at $t + \Delta t$ is as follows

$$[M]\{\ddot{q}\}_{t+\Delta t} + [K_T(q)]_t\{\Delta q\} = \{F\}_{t+\Delta t} - [N(q)\{q\}]_t \quad (31)$$

Applying Newmark's numerical integration scheme, Eq. (31) is transformed into a linear algebraic system of equations as

$$[\bar{K}]\{\Delta q\} = \{\bar{F}\} \quad (32a)$$

where

$$[\bar{K}] = a_0[M] + [K_T(q)]_t$$

$$\{\bar{F}\} = \{F\}_{t+\Delta t} + [M]\{a_2\{\dot{q}\}_t + a_3\{\ddot{q}\}_t\} - \left\{[N(q)]\{q\}\right\}_t$$

$$a_0 = 1/\beta(\Delta t)^2; a_2 = 1/\beta\Delta t; a_3 = (1/2\beta) - 1 \quad (32b)$$

Here, the constants α and β are parameters that control the stability and accuracy of the numerical scheme respectively. The displacement increment $\{\Delta q\}$ is evaluated from above Eq. (32). Then, the displacement, velocity and acceleration vectors at $t + \Delta t$ can be calculated as below:

$$\{\ddot{q}\}_{t+\Delta t} = a_0\{\Delta q\} - a_2\{\dot{q}\}_t - a_3\{\ddot{q}\}_t \quad (33)$$

$$\{\dot{q}\}_{t+\Delta t} = a_1\{\Delta q\} - a_4\{\dot{q}\}_t - a_5\{\ddot{q}\}_t \quad (34)$$

$$\{q\}_{t+\Delta t} = \{q\}_t + \{\Delta q\} \quad (35)$$

where $a_1 = \alpha/\beta\Delta t; a_4 = (\alpha/\beta) - 1; a_5 = (\Delta t/2)\,(\alpha/\beta - 1)$

To improve the solution accuracy and to prevent numerical instabilities, modified Newton-Raphson iteration scheme is applied to yield equilibrium at the end of every time step until the convergence criteria suggested in Refs. [48] are satisfied within a specified tolerance limit of less than one percent.

5.4. Buckling Criterion

The criterion to estimate the critical buckling load is generally well established for the case of static buckling of axisymmetric shallow spherical shells. However, for predicting the dynamic buckling load, the transient response behaviors of the shell for various load amplitudes are necessary. In general, the dynamic buckling criterion

proposed by Budiansky and Roth [2] is accepted. This criterion gives reasonably agreed results when employed with different numerical techniques. By this criterion, the maximum non-dimensional average displacement and central displacement from the transient analysis against the amplitude of pressure load are to be estimated. The dynamic buckling or snap–through buckling load is related to the point of inflection in the load-deflection curve wherein a sudden jump in peak average or central displacement is noticeable for a very small increment in load magnitude [49].

6. Results and Discussions

The problem considered in this paper is that of the nonlinear dynamic buckling of curved classical and non-classical beam, viz., macro and nanobeams, under the influence of a suddenly applied transverse step load. This paper aims firstly in revisiting the problem done earlier and to provide rich data followed by an extensive modal analysis of the trends in the critical buckling load of curved beams. Next, the size dependent effect of non-classical beam through nonlocal model is focused. To ensure the efficiency of the model and exactness of the results, the finite element formulation here is subjected to a progressive mesh refinement process against finding out the non-dimensional critical buckling load $P_{cr} = \frac{R^2 p}{h^2 E}$ for various configurations of the curved beam, toggled by the geometric parameter λ defined as equal to $\frac{R\theta}{4h}$. The geometric parameter λ variation allows one to understand the behavior of curved beam which can be either thick/thin, and/or shallow/deep. Since the present work is dynamic in nature, carrying out *a posteriori* modal decomposition of the registered response using the modal expansion approach [50] sheds light on the participation of various natural modes. Therefore, the mesh based convergence of the first eight dimensionless natural frequencies, $\bar{\omega}_i = \omega_i L^2 \sqrt{\frac{m}{EI}}$ where $m = \rho h$ & $I = \frac{h^3}{12}$ is provided along with P_{cr} in Table 1. To ensure the versatility of the model, beams subjected to two different boundary conditions, hinged-hinged (*HH*) and clamped-clamped (*CC*) are considered. The results computed for different beam geometries ($\lambda = \{5,10,20\}$), as seen from Table 1, show that a curved beam approximated using 32-elements idealization reports

converged results and the same is used for all the subsequent analysis. Unless otherwise mentioned, the applied step load is retained over the beam for infinite duration.

The identification of the critical dynamic buckling load using the criterion outlined in [2, 49] requires the careful analysis of the nonlinear transient response for a range of loads as the minimum load corresponding to a sudden spike in the deflection is treated as the critical buckling load. To ensure the accuracy of the time response, the parameters α and β in the Newmark's integration scheme are taken as 0.5 and 0.25, which correspond to an unconditionally stable scheme. The critical time step of a conditionally stable finite difference scheme, proposed by Leech [51], and Tsui and Tong [52], was computed. Furthermore to choose a time increment that guarantees a stable result, a convergence study was carried. The initial displacement and velocity vectors are assumed to be zero. The non-dimensional time $\tau = \frac{ct}{R}$, (where $c = \sqrt{\frac{E}{\rho}}$ is the speed of sound in material) runs till 120, which is large enough to allow deflection-time curve to develop fully and small enough in real time ($\approx 10^{-6}s$) to ensure the structural resilience. The $\Delta\tau$ chosen adopting the convergence study is the order of 0.005 which is comparable with the critical time step computed for a conditionally stable finite difference scheme [51, 52].

6.1 Classical curved beam (μ= 0)

The validation of the nonlinear formulation is established against the work done by Humphreys [7] for a classical hinged-hinged curved beam. The critical load, for instance, $\lambda = 15$ is traced from the response of the structure under three different loadings as highlighted in Fig. 3a, where at $P_{cr} = 0.126$ the beam undergoes a sudden large displacement, which is evident in the max-displacement versus the load plot, see the inset picture. Following such studies in time domain, the dynamic snap-through loads evolved with respect to the geometric parameter are displayed in Fig. 3b including the analytical results of Humphreys [7]. The numerical data pertaining to Fig. 3(b) is also tabulated in Table 2 to benchmark for assessing other theories and solution methodology. It can be seen in this Figure and Table that the decreasing trend in dynamic buckling loads is observed against a wide range of the beam geometry. The finite element solutions presented here agree fairly well for geometric parameter λ up to certain value, beyond which higher critical values are predicted. The small discrepancy in results for lower beam geometry parameter and large disparity for higher λ are possibly attributed to the different beam theories and

solution procedures employed in Ref. [7] and in the present approach as well. The analysis in Ref. [7] was based on the beam shallowness assumption leading to constant resultant membrane force and neglecting both in-plane inertia and transverse shear deformation effects. Furthermore, the governing equations were solved assuming *a priori* few linear natural modes of the flat beam which are quite different from the free vibration mode shapes of curved beam. The present model accounts for all the inertia terms and higher-order formulation capturing the influence of thick & deep beams. The solutions are evaluated numerically without introducing the natural modes but the various participations of natural modes are extracted from the total response. The proposed formulation is also validated against the dynamic buckling simply supported isotropic and graphene reinforced composite arches [53,16] subjected to centrally applied point load, P_p. It is seen from Fig. [4] that the present results are in very good agreement with the analytical solutions of Ref. [53]. The graphene reinforced composite curved beam case is tested for a selected geometric parameter ($\lambda = 10$) by evaluating the material properties based on Ref. [54] and then the critical dynamic buckling loads calculated by varying the weight fraction of graphe platelets content (W_{gpl}) are compared against the available results in Ref. [16] in Table 3 and they are found to be in excellent agreement with the analytical results..

To investigate the nature and degree of participation of various modes in the nonlinear response, knowledge on the free vibration mode shapes of curved beam is essential; hence, for instance, the first ten normalized eigen modes obtained from the free vibration analysis of hinged-hinged curved beam with $\lambda = \{5,10\}$ are depicted in Fig. 5. Here, each mode is identified by the harmonic waves and their nature in the sense whether they are qualitatively symmetric (*S*) or sort of asymmetric (*A*) with respect to beam geometry, for example, 1*S*, 2*S* here stand for the first and second symmetric modes whereas 1*A* & 2*A* refer the first and second asymmetric cases. A few special cases however occurs, such as 2*S*-(*a*) for $\lambda = 5$ & 2*S*-(*b*) for $\lambda = 10$, resembling sort of second symmetric mode but the outward and inward travel of the modes are quite different; the mode 2*S*-(*b*) appears like a double frequency breathing mode quite common in nonlinear vibration of closed ring or shell structures [50]. It is clear from this discussion that, unlike in the case of flat beam, the eigen modes for the curved beam cases are quite different in terms of the nature of the waves; peak deflection of the wave on either direction of motion of beam can be different, depending beam geometry parameter. This is the reason for the under- or over-estimation of critical loads based on

analytical approach with assumed mode solutions. It can be noted here that the identification of natural modes, viz., 1*S*, 1*A*, 2S-(a) and-(b), etc. can also be done for clamped-clamped (*CC*) as that of hinged-hinged (*HH*) case; however, such labeling, in a similar sense qualitatively, can be followed for clamped-hinged (*CH*) case as the end conditions are different. For the sake brevity, such mode plots are not shown here.

Fig. 6 exhibits the level of participation of various natural modes such as 1*S*, 1*A*, 2*S*, etc. in terms modal participation factor Δ_i^* using the global time response of hinged-hinged curved beams with $\lambda = \{5,10,20\}$ at the critical loads; these factors are found by applying the modal expansion approach using the normalized free vibration modes. For the low value of λ mainly associated with thick/shallow case, it is noticed that the first two symmetric modes 1*S* & 2*S*-(*a*) get excited along with a few asymmetric modes. The total response is significantly dominated by the participation of 1S, and less by 2*S*-(*a*) which is rather out of phase with the 1*S* mode. It is further viewed that, for the moderately thin/deep beam, the active involvement of lower symmetric mode is absent, and all the higher symmetric modes take part in the response and are in same phase; most prevalent mode is 2S-(*b*), followed by 2*S*-(*a*) and then mode 3*S*. However, for very deep curved beam, although the higher modes dictate the response of the beam, the action of very high modes among the participation modes can be out of phase with other modes. It can be concluded that the lower-order symmetric modes are responsible for buckling of shallow geometry whereas the higher symmetric eigen modes pronounce the snap-through load in deep beam. It can be further opined that more energy imparted by the participating modes initiates dynamic instability early at low load. However, the way these modes take part in the response can affect the magnitude of the critical loads.

Next, the influence of other boundary conditions on the dynamic buckling of beams and the contributing natural modes for the response of the structures is thoroughly investigated. Fig. 7b shows the variation of the critical loads with the geometric parameter λ for the clamped-clamped beam assessed from the global time response *viz*., following a typical time response & the related load-deflection plot, see Fig. 7a for $\lambda = 19$. The trend in the snap-through with respect to geometry parameter is qualitatively similar to that of hinged-hinged case. The modal participation factors connected with various natural modes can be noticed in Fig. 8 for the selected geometric parameter. It reveals that, for the geometry up to moderately deep case $\lambda \leq 10$, P_{cr} is lower for clamped beam than that of the hinged-hinged beam. This is due to the overall energy imparted by the modes participation during the

response time on the structure is high for *CC* case compared with those of *HH* case (Fig 6). Also, it appears there is no active participation of asymmetric modes for shallow clamped beam as opposed to the case of *HH* beam. For very deep case, unlike in *HH* case, all higher symmetric modes are in same phase while contributing to the response, and the model participation factor of the most prevalent mode 2*S*-(*b*) is more than that of the *HH* case. The nonlinear dynamic study carried out for clamped-hinged curved beam is presented in terms of P_{cr} versus λ as plotted in Fig. 9b. It is observed that P_{cr} for the *CH* beam is in general lower than those of both the *CC* and *HH* cases and this is mainly due to significant participation of all the modes (as per classification by qualitatively near to symmetric, *S* and asymmetric, *A* modes) as exhibited in Fig. 10. The occurrence of asymmetric modes in the global response is quite obvious as the beam end supports are not symmetric. It can also be seen that the higher energy is imparted to beam through the nearly symmetric, and asymmetric modes at any instant of response time compared to those of other boundary conditions, thus effectively reducing the buckling load. The mode like 2S- (a) & (b) usually do not appear in flat beam case.

In practice, the geometry imperfection due to manufacturing process and initial conditions in dynamic problem can drastically affect the load carrying capacity of the structural system. Some study considering the initial conditions in the form of mode shapes and varying its amplitude is conducted on the dynamic snap-through of simply supported beams $\lambda = \{5,10\}$ and the results are shown in Fig. 11. It is brought out that the buckling load decreases in general with the increase in initial amplitude, as expected. It is also interpreted from Fig. 11a that, for the geometry $\lambda = 5$ while perturbing through the single mode, the asymmetric mode excitation results in lowering the critical load in comparison with those of symmetric mode case for the initial amplitude up to a moderate level. However, with further increase in amplitude, the difference in the calculated values by these initial disturbances is less. The reason for such behavior is due to the change in the way of participation of both symmetric and asymmetric natural modes in the nonlinear response as discussed in modal participation factors with reference to Figs, 6, 8, and 10. The perturbation through the multi-modes is also examined for $\lambda = 10$ and the predictions are highlighted in Fig. 11b. It is viewed from this Figure that the critical loads are appreciably reduced compared to the single mode cases as seen in Fig. 11a. The extracted modal participation factors are depicted in Fig. 12 for λ=10 and the active engagement of all types modes in the total response is visualized for asymmetric disturbance case

whereas only the symmetric modes take part while considering initial condition through the symmetric multi-modes.

7.2 Non-classical curved beam (nanobeam)

Before proceeding for the detailed nonlocal analysis, the nonlocal nonlinear model derived in Section 3 is tested for the known solved problems available in the literature. In Table 4, the frequencies of the natural modes of curved nanobeam computed here are compared with the analytical solutions based on Timoshenko theory by Hosseini and Rahmani [55] for two values length-to thickness ratio. It can be noted here that they are found to be in close agreement. The small discrepancy in the results is attributed to the difference in theories employed here. Next, the linear transient response study considering suddenly applied sinusoidal load retained over the beam with finite duration (T_F) available in the literature [56] for the curved nanobeam is tested against the present model and the results are depicted in Fig. 13 along with those of the Navier approach; they show very good match. Then, the investigation on the nonlinear transient behavior of non-classical curved beam is conducted as presented in Fig. 14. This Figure compares the linear and nonlinear dynamic responses of a *HH* classical (μ= 0) and non-classical (μ= 4) curved beams with geometrical parameter, λ= 5. The nonlinear response registers a vibration of greater amplitude against the linear analysis and can exhibit a kind of beat phenomenon for the higher nonlocal parameter. The amplitude of vibration rises rapidly with increase in the applied load, which is not appreciable in the linear response case. At critical loads, the linear formulation fails to register a sudden rise in deflection, while the nonlinear formulation is able to update the system with the rapidly increasing membrane force at large deflections. As the system approaches instability, it snaps to another stable configuration, about which it continues vibrating.

Having validated the formulation and studied the nonlocal parameter effect on the transient response, a parametric investigation for dynamic buckling of curved nanobeam under a step load assuming hinged-hinged (*HH*) and clamped-hinged (*CH*) support conditions is made for different values of the nonlocal parameter $\mu = (e_0 a_0)^2$ as $\{0,1,2,3,4\}$ $(nm)^2$. These values are specifically taken because $(e_0 a_0)$ is $\leq$ 2nm as discussed in [43]. The results achieved through the present nonlocal nonlinear formulation are described in Fig.15 for *HH* case. As inferred from this Figure, a decrease in the P_{cr} can be seen with the increase in the nonlocal parameter due to the additional load

and inertia contribution introduced by the way of nonlocal formulation; the critical reduces monotonically and approaches a near constant value with respect to λ. This characteristics of a curved nanobeam is somewhat different from that of classical beam analysis ($\mu = 0$), for higher geometric parameter. A modal expansion approach conducted subsequently for the modal response is provided in Fig. 16 with $\lambda = \{5,10,20\}$ and nonlocal parameter, $\mu = 1$ & $4\ nm^2$. It can be viewed from the investigation of the modal participation that only the higher symmetric modes get excited irrespective shallow or deep beam *HH* case; unlike in local analysis, $\mu = 0$ (Fig. 6), the absence of lowest symmetric mode and asymmetric modes in the response is observed for thick or shallow beam case (λ=5).

Similar study for *CH* non-classical beam is made; the predicted critical values against geometry parameter for different values of nonlocal parameter, and the modal participation factor for the selected geometry $\lambda = \{5,10,20\}$ are shown in Fig.17 and 18, respectively. It is observed that, for higher values of λ, the behavior of CH nanobeam case is qualitatively different, in the sense, that the stability of structure is improved compared to those of hinged-hinged case. Furthermore, the higher modes associated with symmetric and asymmetric take part in the global response (Fig. 18) as experienced in local analysis, $\mu = 0$ (Fig. 10). The consequence of the size-dependent effect is to increase the participation of a greater number of natural modes resulting in lowering the dynamic buckling load of nanobeam.

The same problem is lastly studied to bring out the influence of pulse load with finite duration, τ_p in the form of rectangular in nature by presuming *HH* nanobeam (λ =5). It can be noticed from Fig. 19a that the dynamic buckling load increases rapidly with the decrease in pulse duration, irrespective of the material length parameter, μ. It is further seen that, with the increase in pulse duration, the buckling load approaches asymptotically the value corresponding to a pulse of infinite duration. The modal responses are also shown in Fig. 19b for μ =0 & 1 corresponding to the load duration =2.5 to highlight the nature of different modes in contributing to the buckling response.

7. Conclusion

The nonlocal nonlinear finite element approach for the dynamic analysis of curved beam by integrating the Eringen's nonlocal differential constitutive relations, geometric nonlinearity stemming from moderately large deflection and rotation, and shear deformation SIN model is developed for the first time in predicting the dynamic bucking of curved macro and nanobeams under suddenly applied step loads. The performance of the numerical model is test against the available results in the literature. The nature and the degree of modal participation of various natural modes controlling the global response of the beam are brought out *a posteriori* by modal expansion approach. A comprehensive investigation is made to highlight the influence of various design parameters pertaining to the geometry and nonlocal parameter, initial condition, applied load duration, and boundary conditions on the dynamic snap-through. From the present study, some of the observations made are as follows:

i) Imposing assumed mode shapes for solution based on flat beam can affect the buckling behavior of curved arch with respect to the geometric parameter λ.

ii) The extracted natural modes from the global response using modal expansion approach are qualitatively different from those of flat case.

iii) The lowest fundamental mode mainly gets activated in the transient response analysis for shallow beam.

iv) For thin deep beam, symmetric modes with higher frequencies impart energy to the beam with symmetric supports like *HH* and *CC*.

v) Participation of lower and higher modes, irrespective of the nature of modes, is observed for asymmetric end supports (*CH*) in snap-through buckling.

vi) Unlike static case, the geometry in conjunction with the boundary conditions dictates the level of buckling load.

vii) The symmetric modes labeled with 2*S*(*b*) and (*a*) , in general, dominate the buckling response.

viii) As expected, the nature of initial conditions and its amplitude can predominately affect the load carrying of the structure.

ix) The response amplitude increases with the increase in the nonlocal parameter.

x) With increase in the nonlocal parameter, critical buckling value rapidly reduces initially and then monotonically decreases with the geometric parameter.

xi) Unlike in the case of classical beam, more number of higher modes participation are seen in snap-through response of curved nanobeam resulting in reduction in critical load.

xii) With the reduction in pulse load duration results in rapidly increasing the critical load.

Appendix A

$$\int_0^t \int_0^L \Big[(-N'_{xx} - \tfrac{1}{R}(M'_{xx} - \widehat{M}'_{xx}) - \tfrac{1}{R}\hat{Q}_{xz} - (\widehat{M}'_{xx}\theta' + \widehat{M}_{xx}\theta'') - (\hat{Q}'_{xz}\theta + \hat{Q}_{xz}\theta)\ \Big)\delta u_0 + \Big(\tfrac{1}{R}N_{xx} - (M''_{xx} - \widehat{M}''_{xx}) - \hat{Q}'_{xz} - N_{xx}w''_o - N'_{xx}w'_o\Big)\delta w_0 + \big(-\widehat{M}'_{xx} + \hat{Q}_{xz} - (M^{*'}\theta' + M^*\theta'') - Q^{*'}\theta - (\widehat{M}'_{xx}u'_0 + \widehat{M}_{xx}u''_0) + \hat{Q}_{xz}u'_0\big)\delta\theta - P\delta w_0 - \mu P'\delta w'_0 + \big(I_1\ddot{u}_0 + I_2\ddot{w}'_0 + I_3\ddot{\theta}\big)\delta v_0 - \big(I_2\ddot{u}'_0 + I_4\ddot{w}''_0 + I_5\ddot{\theta}' - I_0\ddot{w}_0\big)\delta w_0 + \big(I_3\ddot{u}_0 + I_5\ddot{w}'_0 + I_6\ddot{\theta}\big)\delta\theta + \mu(I_1\ddot{u}_0{}' + I_2\ddot{w}_0{}'' + I_3\ddot{\theta}')\delta v_0{}' + \mu(I_2\ddot{u}_0{}' + I_4\ddot{w}_0{}'' + I_5\ddot{\theta}')\delta w_0{}'' + \mu(I_3\ddot{u}_0{}' + I_5\ddot{w}_0{}'' + I_6\ddot{\theta}')\delta\theta_0{}' + \mu I_0\ddot{w}_0{}'\delta w_0{}']dxdt + \int_0^t [\bar{N}\delta u_0 + \bar{V}\delta w_0 + \bar{M}\delta w_0{}' + \bar{P}\delta\theta]_0^L dt + \int_0^L [N^T\delta u_0 + V^T\delta w_0 + M^T\delta w_0{}' + P^T\delta\theta]_0^T dx = 0 \quad \text{(A.1)}$$

With the following boundary conditions at the ends of the beam:

$$u_0 \text{ or } \bar{N} + \Big[N_{xx} + \frac{1}{R}(M_{xx} - \widehat{M}_{xx}) + \widehat{M}_{xx}\theta' + \hat{Q}_{xz}\theta - \mu(I_1\ddot{u}_0{}' + I_2\ddot{w}_0{}'' + I_3\ddot{\theta}')\Big]$$

$$w_0 \text{ or } \bar{V} + \big[\hat{Q}_{xz} + M'_{xx} - \widehat{M}'_{xx} + \big(I_2\ddot{u}_0 + I_4\ddot{w}_0{}' + I_5\ddot{\theta}\big) + \mu(P' - I_0\ddot{w}_0{}') + N_{xx}w'_0\big]$$

$$w'_0 \text{ or } \bar{M} + \big[(\widehat{M}_{xx} - M_{xx}) - \mu(I_2\ddot{u}_0{}' + I_4\ddot{w}_0{}'' + I_5\ddot{\theta}')\big]$$

$$\theta \text{ or } \bar{P} + \big[\widehat{M}_{xx} - \mu\big(I_3\ddot{u}_0{}' + I_5\ddot{w}_0{}'' + I_6\ddot{\theta}'\big) + M^*\theta' + Q^*\theta + \widehat{M}_{xx}u'_0\big] \quad \text{(A.2)}$$

With the following initial conditions for the beam:

$$u_0 \text{ or } N^T + [-\big(I_1\dot{u}_0 + I_2\dot{w}'_0 + I_3\dot{\theta}\big) + \mu(I_1\dot{u}_0{}'' + I_2\dot{w}_0{}''' + I_3\dot{w}_0{}'')]$$

$$w_0 \text{ or } V^T + [-I_0\dot{w}_0 + \mu I_0\dot{w}_0{}'']$$

$$w'_0 \text{ or } M^T + [-(I_2\dot{u}_0 + I_4\dot{w}_0{}' + I_5\dot{\theta}) + \mu\big(I_2\dot{u}_0{}'' + I_4\dot{w}_0{}''' + I_5\dot{\theta}''\big)]$$

$$\theta \text{ or } P^T + [\ -\big(I_3\dot{u}_0 + I_5\dot{w}_0{}' + I_6\dot{\theta}\big) + \mu(I_3\dot{u}_0{}'' + I_5\dot{w}_0{}''' + I_6\theta'')] \quad \text{(A.3)}$$

Appendix B

The vectors $\{d\}^T$in terms of derivatives of displacement variables in defining the strain components ε_{xx} & γ_{xz} Eq. (16) defined in Eq. (31) is given here as,

$$\{\mathrm{d}\}^T = \Big[\Big(u'_0 + \tfrac{w_0}{R}\Big) \quad \Big(\tfrac{u'_0}{\mathrm{R}} - w''_0\Big) \quad \Big(w''_0 + \theta' - \tfrac{u'_0}{\mathrm{R}}\Big) \quad \gamma_0 \quad w'_0 \quad \theta \quad \theta' \quad u'_0\Big] \quad \text{(B.1)}$$

Element formulation is derived in general form considering strain-displacement relationship given in Eq. (16) can be written as:

$$\varepsilon_{xx} = \{d\}^T\{L_1\} + \tfrac{1}{2}\{d\}^T[H_1]\{d\}\ ;\ \gamma_{xz} = \{d\}^T\{L_2\} + \tfrac{1}{2}\{d\}^T[H_2]\{d\} \quad \text{(B.2)}$$

where $\{L_i\}$ is the linear strain vector, $[H_i]$ is a symmetric matrix based on linear and nonlinear strain components. These vectors and matrices are defined as

$$[L_1]^T = [1 \quad z \quad f \quad 0 \quad 0 \quad 0 \quad 0 \quad 0] \; ; \; [L_2]^T = [0 \quad 0 \quad 0 \quad f_{,z} \quad 0 \quad 0 \quad 0 \quad 0] \tag{B.3}$$

$$[H_1] = \begin{bmatrix} 0 & 0 & 0 & 0 & 0 & 0 & 0 & 0 \\ 0 & 0 & 0 & 0 & 0 & 0 & 0 & 0 \\ 0 & 0 & 0 & 0 & 0 & 0 & 0 & 0 \\ 0 & 0 & 0 & 0 & 0 & 0 & 0 & 0 \\ 0 & 0 & 0 & 0 & 1 & 0 & 0 & 0 \\ 0 & 0 & 0 & 0 & 0 & 0 & 0 & 0 \\ 0 & 0 & 0 & 0 & 0 & 0 & f^2 & f \\ 0 & 0 & 0 & 0 & 0 & 0 & f & 0 \end{bmatrix}; [H_2] = \begin{bmatrix} 0 & 0 & 0 & 0 & 0 & 0 & 0 & 0 \\ 0 & 0 & 0 & 0 & 0 & 0 & 0 & 0 \\ 0 & 0 & 0 & 0 & 0 & 0 & 0 & 0 \\ 0 & 0 & 0 & 0 & 0 & 0 & 0 & 0 \\ 0 & 0 & 0 & 0 & 0 & 0 & 0 & 0 \\ 0 & 0 & 0 & 0 & 0 & 0 & ff_{,z} & f_{,z} \\ 0 & 0 & 0 & 0 & 0 & ff_{,z} & 0 & 0 \\ 0 & 0 & 0 & 0 & 0 & f_{,z} & 0 & 0 \end{bmatrix} \tag{B.4}$$

The Matrices, $[\hat{K}]$, $[\hat{N}_1]$, $[\hat{N}_2]$ & $[\hat{N}_3]$ defining the strain energy functional Eq. (18) are expressed as [63]

$$[\hat{K}] = [L_1][L_1]^T \tag{B.5a}$$

$$[\hat{N}_1] = \sum_{i=1}^{2} [L_i]\{d\}^T[H_i] + \{d\}^T[L_i][H_i] + [H_i]\{d\}[L_i]^T \tag{B.5b}$$

$$[\hat{N}_2] = \sum_{i=1}^{2} [H_i]\{d\}\{d\}^T[H_i] + \frac{1}{2}\{d\}^T[H_i]\{d\}[H_i] \tag{B.5c}$$

$$[\hat{N}_3] = [L_2][L_2]^T; \tag{B.5d}$$

These matrices thus derived here are given as

$$[\hat{M}] = \int_{-\square/2}^{\square/2} \rho \begin{bmatrix} 1 & z & f & 0 \\ z & z^2 & zf & 0 \\ f & zf & f^2 & 0 \\ 0 & 0 & 0 & 1 \end{bmatrix} dz; \quad [\hat{K}] = \int_{-h/2}^{h/2} C_{11} \begin{bmatrix} 1 & z & f & 0 & 0 & 0 & 0 & 0 \\ z & z^2 & zf & 0 & 0 & 0 & 0 & 0 \\ f & zf & f^2 & 0 & 0 & 0 & 0 & 0 \\ 0 & 0 & 0 & 0 & 0 & 0 & 0 & 0 \\ 0 & 0 & 0 & 0 & 0 & 0 & 0 & 0 \\ 0 & 0 & 0 & 0 & 0 & 0 & 0 & 0 \\ 0 & 0 & 0 & 0 & 0 & 0 & 0 & 0 \\ 0 & 0 & 0 & 0 & 0 & 0 & 0 & 0 \end{bmatrix} dz$$

(B.6a)

$$[\widehat{N}_1] =$$

$$\int_{-h/2}^{h/2} \begin{bmatrix} 0 & 0 & 0 & 0 & (w'_0)C_{11} & 0 & (f^2\theta' + fu'_0)C_{11} & (f\theta')C_{11} \\ 0 & 0 & 0 & 0 & (zw'_0)C_{11} & 0 & z(f^2\theta' + fu'_0)C_{11} & (zf\theta')C_{11} \\ 0 & 0 & 0 & 0 & (fw'_0)C_{11} & 0 & f(f^2\theta' + fu'_0)C_{11} & (f^2\theta')C_{11} \\ 0 & 0 & 0 & 0 & 0 & (\theta' ff_{,z} + f_{,z}u'_0)C_{66} & (\theta ff_{,z})C_{66} & (\theta f_{,z})C_{66} \\ (w'_0)C_{11} & (zw'_0)C_{11} & (fw'_0)C_{11} & 0 & \varepsilon^L_{xx}C_{11} & 0 & 0 & 0 \\ 0 & 0 & 0 & (\theta' ff_{,z} + f_{,z}u'_0)C_{66} & 0 & 0 & (\gamma_0 ff_{,z})C_{66} & (\gamma_0 f_{,z})C_{66} \\ (f^2\theta' + fu'_0)C_{11} & z(f^2\theta' + fu'_0)C_{11} & f(f^2\theta' + fu'_0)C_{11} & (\theta ff_{,z})C_{66} & 0 & (\gamma_0 ff_{,z})C_{66} & f^2\varepsilon^L_{xx}C_{11} & f\varepsilon^L_{xx}C_{11} \\ (f\theta')C_{11} & (zf\theta')C_{11} & (f^2\theta')C_{11} & (\theta f_{,z})C_{66} & 0 & (\gamma_0 f_{,z})C_{66} & f\varepsilon^L_{xx}C_{11} & 0 \end{bmatrix} dz \quad \text{(B.6b)}$$

$$[\widehat{N}_2] =$$

$$\int_{-h/2}^{h/2} \begin{bmatrix} 0 & 0 & 0 & 0 & 0 & 0 & 0 & 0 \\ 0 & 0 & 0 & 0 & 0 & 0 & 0 & 0 \\ 0 & 0 & 0 & 0 & 0 & 0 & 0 & 0 \\ 0 & 0 & 0 & 0 & 0 & 0 & 0 & 0 \\ 0 & 0 & 0 & 0 & \left(\frac{3}{2}w'^2_0 + \frac{1}{2}(f\theta')^2 + fu'_0\theta'\right)C_{11} & 0 & w'_0(f^2\theta' + fu'_0)C_{11} & (f\theta'w'_0)C_{11} \\ 0 & 0 & 0 & 0 & 0 & (\theta' ff_{,z} + f'u'_0)^2 C_{66} & 2(\theta\theta'(ff_{,z})^2 + \theta f(f')^2u'_0)\, C_{66} & 2(\theta\theta' f(f_{,z})^2 + \theta(f')^2u'_0)\, C_{66} \\ 0 & 0 & 0 & 0 & w'_0(f^2\theta' + fu'_0)C_{11} & 2(\theta\theta'(ff_{,z})^2 + \theta f(f')^2u'_0)\, C_{66} & C_{11}\left(\frac{1}{2}(fw'_0)^2 + \frac{3}{2}(f^2\theta')^2 + f^2u'^2_0 + 3f^3\theta'u'_0\right) + C_{66}(\theta ff_{,z})^2 & C_{11}\left(\frac{1}{2}fw_0^2 + \frac{3}{2}f^3\theta'^2 + 2f^2\theta'u'_0\right) + f(\theta f')^2C_{66} \\ 0 & 0 & 0 & 0 & (f\theta'w'_0)C_{11} & 2(\theta\theta' f(f_{,z})^2 + \theta(f')^2u'_0)\, C_{66} & C_{11}\left(\frac{1}{2}fw_0^2 + \frac{3}{2}f^3\theta'^2 + 2f^2\theta'u'_0\right) + f(\theta f')^2C_{66} & C_{11}(f\theta')^2 + C_{66}(\theta f')^2 \end{bmatrix} dz$$

$$[\widehat{N}_3] = \int_{-h/2}^{h/2} C_{66} \begin{bmatrix} 0 & 0 & 0 & 0 & 0 & 0 & 0 & 0 \\ 0 & 0 & 0 & 0 & 0 & 0 & 0 & 0 \\ 0 & 0 & 0 & 0 & 0 & 0 & 0 & 0 \\ 0 & 0 & 0 & (f_{,z})^2 & 0 & 0 & 0 & 0 \\ 0 & 0 & 0 & 0 & 0 & 0 & 0 & 0 \\ 0 & 0 & 0 & 0 & 0 & 0 & 0 & 0 \\ 0 & 0 & 0 & 0 & 0 & 0 & 0 & 0 \\ 0 & 0 & 0 & 0 & 0 & 0 & 0 & 0 \end{bmatrix} dz \quad \text{(B.6c&d)}$$

References

[1] George J. Simitses, 1990. Dynamic Stability of Suddenly Loaded Structures, Springer-Verlag New York VIII, 290. 10.1007/978-1-4612-3244-5

[2] B. Budiansky, R.S. Roth, Axisymmetric dynamic buckling of clamped shallow spherical shells, Collected Papers on Instability of Shell Structures. NASA TN D-151O, (1962).

[3] N.J. Hoff, V.C. Bruce, Dynamic analysis of the buckling of laterally loaded flat arches, Journal of Mathematics and Physics. 32 (1954) 276-388. https://doi.org/10.1002/sapm1953321276

[4] N. C. Huang,W. Nachbar, Dynamic snap-through of imperfect viscoelastic shallow arches, Journal of Applied Mechanics. 35 (1968) 289-296. https://doi.org/10.1115/1.3601194

[5] G.A. Hegemier, F. Tzung, Influence of damping on the snapping of a shallow arch under a step pressure load, AIAA Journal. 7 (1969) 1494-1499. https://doi.org/10.2514/3.5421

[6] C.S. Hsu, C.T. KUO, R.H. Plaut, Dynamic stability criteria for clamped shallow arches under time wise step loads, AIAA Journal. 7 (1969) 1925-193. https://doi.org/10.2514/3.5483

[7] John S. Humphreys, On dynamic snap buckling of shallow arches, AIAA journal. 4 (1966) 878-886. https://doi.org/10.2514/3.3561

[8] W.Y. Poon, C.F Ng, Y.Y. Lee, Dynamic stability of a curved beam under sinusoidal loading, Proceedings of the Institution of Mechanical Engineers, Part G: Journal of Aerospace Engineering, 216 (2002) 209-217. https://doi.org/10.1243/09544100260369740

[9] J.S Lin, J.S Chen, Dynamic snap-through of a laterally loaded arch under prescribed end motion, International journal of solids and structures. 40 (2003) 4769-4787. https://doi.org/10.1016/S0020-7683(03)00181-1

[10] J.S. Chen, W.C. Ro, J.S. Lin, Exact static and dynamic critical loads of a sinusoidal arch under a point force at the midpoint, International Journal of Non-Linear Mechanics. 44 (2009) 66-70. https://doi.org/10.1016/j.ijnonlinmec.2008.08.006

[11] Y. Chen, J. Feng, Elastic stability of shallow pin-ended parabolic arches subjected to step loads, Journal of Central South University of Technology. 17 (2010) 156-162. https://doi.org/10.1007/s11771-010-0025-3

[12] A. Abdelgawad, A. Anwar, M. Nassar, Snap-through buckling of a shallow arch resting on a two-parameter elastic foundation, Applied Mathematical Modelling. 37 (2013) 7953-7963. https://doi.org/10.1016/j.apm.2013.03.016

[13] I. Sheinman, Dynamic large-displacement analysis of curved beams involving shear deformation, International Journal of Solids and Structures. 16 (1980) 1037-1049. https://doi.org/10.1016/0020-7683(80)90103-1

[14] L.S. Chien, A.N. Palazotto, Dynamic buckling of composite cylindrical panels with high-order transverse shears subjected to a transverse concentrated load, International journal of non-linear mechanics. 27 (1992) 719-734. 10.1016/0020-7462(92)90029-7

[15] Y.L. Pi, M.A. Bradford, Nonlinear dynamic buckling of shallow circular arches under a sudden uniform radial load, Journal of Sound and Vibration. 331 (2012) 4199-4217. https://doi.org/10.1016/j.jsv.2012.04.015

[16] Z. Yang, A. Liu, J. Yang, J. Fu, B. Yang, Dynamic buckling of functionally graded graphene nanoplatelets reinforced composite shallow arches under a step central point load, Journal of Sound and Vibration. 465 (2020) 115019. https://doi.org/10.1016/j.jsv.2019.115019

[17] Y. Chandra, R. Wiebe, I. Stanciulescu, L.N. Virgin, S.M. Spottswood, T.G. Eason, Characterizing dynamic transitions associated with snap-through of clamped shallow arches, Journal of Sound and Vibration. 332 (2013) 5837-5855. https://doi.org/10.1016/j.jsv.2013.06.001

[18] S.E. Ghiasian, Y. Kiani, R. Eslami, Nonlinear thermal dynamic buckling of FGM beams, European Journal of Mechanics-A/Solids. 54 (2015) 232-242. https://doi.org/10.1016/j.euromechsol.2015.07.004

[19] X. Kong, B. Wang, J. Hu, Dynamic snap buckling of an elastoplastic shallow arch with elastically supported and clamped ends, Computers & structures. 55 (1995) 163-166. https://doi.org/10.1016/0045-7949(94)00416-Z

[20] W.L Fernandes, D.B. Vasconcellos, M. Greco, Dynamic Instability in Shallow Arches under Transversal Forces and Plane Frames with Semirigid Connections, Mathematical Problems in Engineering. 2018 (2018) 1985907. https://doi.org/10.1155/2018/1985907

[21] P. Maharana, J. Sonawane. P. Belehalli, G . K. Anathasuresh, Analysis of Planar Bistable and Snap-through Arches for Contact and Dynamic Loads, In IFToMM World Congress on Mechanism and Machine Science, Springer, Cham. (2019) 3245-3254. https://doi.org/10.1007/978-3-030-20131-9_320

[22] N.J. Mallon, R.H.B. Fey, H. Nijmeijer, G.Q. Zhang, Dynamic buckling of a shallow arch under shock loading considering the effects of the arch shape. International Journal of Non-Linear Mechanics. 41 (2006) 1057-1067. https://doi.org/10.1016/j.ijnonlinmec.2006.10.017

[23] M. Jabareen, I. Sheinman, Dynamic buckling of a beam on a nonlinear elastic foundation under step loading, Journal of Mechanics of Materials and Structures. 4 (2009) 1365-1373. 10.2140/jomms.2009.4.1365

[24] M. Aydogdu. A general nonlocal beam theory: its application to nanobeam bending, buckling and vibration. Physica E 2009:41(9);1651–1655. https://doi.org/10.1016/j.physe.2009.05.014

[25] J.N. Reddy. Nonlocal theories for bending, buckling and vibration of beams. Int. J. Eng. Sci. 2007: 45(2-8);288–307. https://doi.org/10.1016/j.ijengsci.2007.04.004

[26] H.-T. Thai. A nonlocal beam theory for bending, buckling, and vibration of nanobeams. Int. J. Eng. Sci. 2012:52;56–64. https://doi.org/10.1016/j.ijengsci.2011.11.011

[27] Wang, C. M., Y. Y. Zhang, and X. Q. He. "Vibration of nonlocal Timoshenko beams." Nanotechnology 18.10 (2007): 105401. https://doi.org/10.1088/0957-4484/18/10/105401

[28] Ganapathi, M., T. Merzouki, O. Polit. "Vibration study of curved nanobeams based on nonlocal higher-order shear deformation theory using finite element approach." Composite Structures 184 (2018): 821-838. 10.1016/j.compstruct.2017.10.066

[29] Ghayesh, Mergen H., Marco Amabili, and Hamed Farokhi. "Nonlinear forced vibrations of a microbeam based on the strain gradient elasticity theory." International Journal of Engineering Science 63 (2013): 52-60. https://doi.org/10.1016/j.ijengsci.2012.12.001

[30] Ghayesh, Mergen H., Hamed Farokhi, and Marco Amabili. "Nonlinear dynamics of a microscale beam based on the modified couple stress theory." Composites Part B: Engineering 50 (2013): 318-324. https://doi.org/10.1016/j.compositesb.2013.02.021

[31] K. Das, R.C. Batra, Symmetry breaking, snap-through and pull-in instabilities under dynamic loading of microelectromechanical shallow arches, Smart Materials and Structures. 18 (2009) 115008. https://doi.org/10.1088/0964-1726/18/11/115008

[32] K. Das, R.C. Batra, Pull-in and snap-through instabilities in transient deformations of microelectromechanical systems, Journal of Micromechanics and Microengineering. 19 (2009) 035008. https://doi.org/10.1088/0960-1317/19/3/035008

[33] C.M. Wang, Y. Xiang, J. Yang, S. Kitipornchai, Buckling of nano-rings/arches based on nonlocal elasticity, International Journal of Applied Mechanics. 4 (2012) 1250025. https://doi.org/10.1142/S1758825112500251

[34] Kaviani, F., & Mirdamadi, H. R. Snap-through and bifurcation of nano-arches on elastic foundation by the strain gradient and nonlocal theories. International Journal of Structural Stability and Dynamics, 13(05) ., 1350022. (2013) DOI: 10.1142/S0219455413500223

[35] G.L. She, Y.R. Ren, K.M. Yan, On snap-buckling of porous FG curved nanobeams, Acta Astronautica. 161 (2019) 475-484. https://doi.org/10.1016/j.actaastro.2019.04.010

[36] A.C. Eringen, D.G.B. Edelen, On nonlocal elasticity, Int. J. Eng. Sci. 10 (1972) 233–248. https://doi.org/10.1016/0020-7225(72)90039-0

[37] M. Ganapathi and O. Polit, A nonlocal higher-order model including thickness stretching effect for bending and buckling of curved nanobeams, Applied Mathematical Modelling. 57 (2018) 121-141. https://doi.org/10.1016/j.apm.2017.12.025

[38] M. Touratier, An efficient standard plate theory, International Journal of Engineering Science. 29 (1991) 901–916. https://doi.org/10.1016/0020-7225(91)90165-Y

[39] O. Polit, M. Touratier, A multilayered/sandwich triangular finite element applied to linear and non-linear analyses. Compos Struct. 58 (2002) 121–128. https://doi.org/10.1016/S0263-8223(02)00033-8

[40]. C. T. Sun, On the equations for Timoshenko beam under initial stress, ASME J App. Mech. 39 (1972) 82-85. https://doi.org/10.1115/1.3422632

[41] A.C. Eringen, On differential equations of nonlocal elasticity and solutions of screw dislocation and surface waves, J. Appl. Phys. 54 (1983) 4703–4710. https://doi.org/10.1063/1.332803

[42] R. Aghababaei, J.N. Reddy, Nonlocal third-order shear deformation plate theory with application to bending and vibration of plates, Journal of Sound and Vibration. 326 (2009) 277–289. https://doi.org/10.1016/j.jsv.2009.04.044

[43] Q. Wang, Wave propagation carbon nanotubes via nonlocal continuum mechanics, J. Appl. Phys. 98 (2005) 124301. https://doi.org/10.1063/1.2141648

[44] M. Ganapathi, T. K. Varadan, Nonlinear free flexural vibrations of laminated circular cylindrical shells, Compos Struct. 30 (1995)30:33-49. https://doi.org/10.1016/0263-8223(94)00025-5

[45]. C.Ramesh Babu, G. Prathap, A linear thick curved beam element, International Journal for Numerical Methods in Engineering. 23 (1986) 1313–1328. https://doi.org/10.1002/nme.1620230709

[46]. S.Aditya, M. Haboussi, S. Shubhendu, M. Ganapathi, O. Polit, Supersonic flutter study of porous 2D curved panels reinforced with graphene platelets using an accurate shear deformable finite element procedure, Composite Structures. 241 (2020) 112058. doi:10.1016/j.compstruct.2020.112058.

[47] M. Ganapathi, T. K. Varadan, Application of a field-consistent shear flexible element for nonlinear dynamic analysis of laminated shells, Finite Elements in Analysis and Design. 12 (1992) 105-116. https://doi.org/10.1016/0168-874X(92)90058-K

[48] Bergan PG, Clough RW. Convergence criteria for iterative process, Am Inst Aeronautics Astronautics J. 10 (1972) 1107-1108. https://doi.org/10.2514/3.50313

[49]. M. Ganapathi and T. K. Varadan, Dynamic Buckling of Laminated Anisotropic Spherical Caps, ASME, Journal of Applied Mechanics. 62 (1995) 13-19. https://doi.org/10.1115/1.2895879

[50] B. P. Patel, M. Ganapathi, D. P. Makhecha, P. Jha, Large amplitude free flexural vibration of rings using finite element approach, Int. J. Nonlinear Mechanics, 37 (2003) 911-921. https://doi.org/10.1016/S0020-7462(02)00037-9

[51] Leech, J. N., "Stability of Finite Difference Equations for the Transient Response of a Flat Plate," American Institute of Aeronautics and Astronautics Journal, Vol. 3 (1965), pp. 1772-1773. https://doi.org/10.2514/3.55195

[52] Tsui, T. Y., and Tong, P., "Stability of Transient Solution of Moderately Thick Plate by Finite Difference Method," American Institute of Aeronautics and Astronautics Journal, Vol. 9 (1971) pp. 2062-2063. 10.2514/3.6463

[53] Pi, Yong-Lin, and Mark Andrew Bradford. "Dynamic buckling of shallow pin-ended arches under a sudden central concentrated load." Journal of Sound and Vibration 317.3-5 (2008): 898-917. https://doi.org/10.1016/j.jsv.2008.03.037

[54]B. Anirudh, T. Ben Zineb, O. Polit, , M. Ganapathi, G. Prateek, Nonlinear bending of functionally graded graphene platelets reinforced porous composite curved beams using finite element based on trigonometric shear deformation theory, Int. J. Nonlinear Mechanics, Vol. 119 (2020) https://doi.org/10.1016/j.ijnonlinmec.2019.103346 (2019).

[55] S.A.H. Hosseini, O. Rahmani. Free vibration of shallow and deep curved FG nanobeam via nonlocal Timoshenko curved beam model. Appl. Phys. A, 122(2016), 1–11. 10.1007/s00339-016-9696-4

[56] M. Ganapathi, O. Polit. Dynamic characteristics of curved nanobeams using nonlocal higher-order curved beam theory. Physica E: Low-Dim. Sys. and Nanostructures, 91(2017) 190-202. https://doi.org/10.1016/j.physe.2017.04.012.

Legends Tables

Table 1: Convergence study for non-dimensional natural frequency (ϖ) and non-dimensional dynamic critical load (P_{cr}) for different geometric parameters (λ) of classical curved beam. ($\bar{\omega}_i = \omega l^2\sqrt{\frac{m}{EI}}$)

Table 2: Comparison of dynamic buckling loads against geometric parameter ($\boldsymbol{\lambda}$) for *HH* classical for the present study with analytical solutions [7].

Table 3: Comparison of critical dynamic buckling load $\bar{P}_{cr}$ of *HH* classical graphene platelets reinforced composite curved beam under centrally applied point load $P_p$with Ref [16] ($\bar{P} = \frac{P_p}{N_{E0}\theta}$; $N_{E0} = \frac{(1.4303\pi)^2 Ebh^3}{3L^2}$, $\frac{L}{h} = 50, \lambda = 10, W_{gpl} = 0.1\%$).

Table 4: Comparison of non-dimensional natural frequencies of *HH* non-classical curved beam ($\phi = 60°$) for different nonlocal parameter ($\boldsymbol{\mu}$) against analytical solutions [55].($\bar{\omega}_i = \omega l^2\sqrt{\frac{m}{EI}}$)

Legends Figures

Fig.1: a) Geometrical parameters of curved beam b) Beam element with the degrees of freedom.

Fig.2. Un-deformed and deformed geometry of a beam section: (a) un-deformed; (b) Euler-Bernoulli; (c) Timoshenko; (d) higher order theories

Fig. 3a: The load versus time response of classical *HH* curved Beam for $\lambda = 15$.

Fig. 3b: Variation of dynamic critical load against geometric parameter ($\boldsymbol{\lambda}$) for *HH* classical curved beam along with Ref. [7].

Fig. 4: Variation of dynamic critical load $\bar{P}_{cr}$ with geometric parameter λ for HH classical isotropic curved beam under centrally applied point load P_p along with Ref. [53] ($\bar{P}_{cr} = \frac{P_p L^2}{8EI}$).

Fig.5: Representation of different types of natural free vibration mode shapes of *HH* classical curved beam with geometric parameter, $\lambda = 5$ &10

Fig.6: Modal participation factors for HH classical curved beam with $\boldsymbol{\lambda}$ =5, 10 & 20, and at certain loads, *P*.

Fig.7a: The load versus time response of *CC* classical curved Beam for $\lambda = 19$.

Fig. 7b: Variation of dynamic critical load against geometric parameter ($\boldsymbol{\lambda}$) for *CC* classical curved beams.

Fig.8: Modal participation factors for *CC* classical curved beam with $\boldsymbol{\lambda}$ =5, 10 & 20, and at certain loads, P.

Fig.9a: The load versus time response of *CH* classical curved Beam for $\lambda = 4.6$.

Fig.9b: Variation of dynamic critical load against geometric parameter (λ) for CH classical curved beams.

Fig.10: Modal participation factors for *CH* classical curved beam with $\boldsymbol{\lambda}$ =5, 10 & 20, and at certain loads, P.

Fig. 11: Variation of dynamic critical load against initial amplitude, ($\bar{w}_0$) for *HH* classical curved beam with $\boldsymbol{\lambda}$ =5 & 10 (a) single mode perturbation; (b) multi-modes perturbation

Fig. 12: Modal participation factors for *HH* classical curved beam with $\boldsymbol{\lambda}$ =10, and initial amplitude ($\bar{w}_0 = \mathbf{0.1}$) at certain loads, P: (a) symmetric multi-modes perturbation; (b) asymmetric multi-modes perturbation.

Fig. 13: Comparison of linear transient response of *HH* non-classical thick curved beam (*L/h*=5) with analytical solutions [56]: shallow nanobeam, (a) $\varphi = 15°$; (b) deep nanobeam, $\varphi = 120°$.

Fig. 14: Linear and nonlinear transient behavior *HH* non-classical curved beam ($\boldsymbol{\lambda}$ =5) with different nonlocal parameter: (i) $\mu = 0$; (i) $\mu = 4$

Fig.15: Variation of dynamic critical load against geometric parameter ($\boldsymbol{\lambda}$) for *HH* non-classical curved beams with different nonlocal parameter (μ)

Fig. 16: Modal participation factors for HH non-classical curved beam with $\boldsymbol{\lambda}$ =5, 10 & 20, and at certain load, P: (i) μ=1; (ii) μ=4

Fig. 17: Variation of dynamic critical load against geometric parameter ($\boldsymbol{\lambda}$) for *CH* non-classical curved beams with different nonlocal parameter (μ)

Fig. 18: Modal participation factors for *CH* non-classical curved beam with $\boldsymbol{\lambda}$ =5, 10 & 20, and at certain load, P: (i) μ=1; (ii) $\mu = 4$.

Fig. 19: Variation of dynamic critical load and modal responses for *HH* non-classical curved beams $\boldsymbol{\lambda}$ =5 with finite pulse load duration (τ_p): (a) P versus τ_p; (b) Modal response for pulse load duration τ_p=2.5 ($\mu = 0$ & 1).

Table 1: Convergence study for non-dimensional natural frequency (ϖ) and non-dimensional dynamic critical load (P_{cr}) for different geometric parameters (λ) of classical curved beam. ($\bar{\omega}_i = \omega_i L^2 \sqrt{\frac{m}{EI}}$)

B.C	λ	Elements	Non-Dimensional Natural Frequencies								P_{cr}
			$\overline{\omega_1}$	$\overline{\omega_2}$	$\overline{\omega_3}$	$\overline{\omega_4}$	$\overline{\omega_5}$	$\overline{\omega_6}$	$\overline{\omega_7}$	$\overline{\omega_8}$	
	5	4	39.6755	60.4109	94.5984	175.5863	276.1307	430.9504	627.1311	637.2797	0.213
		8	39.1351	60.0812	92.7761	157.0395	246.1253	354.9847	486.1899	626.3690	0.213
		16	39.0969	60.0579	92.6291	156.3681	243.9216	349.0311	472.8827	612.0253	0.214
		32	39.0944	60.0564	92.6193	156.3232	243.7703	348.6068	471.8619	610.0842	0.213
		64	39.0942	60.0563	92.6187	156.3204	243.7606	348.5794	471.7953	609.9545	0.213
HH	10	4	40.9667	85.1644	135.9531	183.4635	285.2159	443.2563	658.4954	797.2291	0.184
		8	39.2878	81.4309	135.6008	158.3340	250.3289	360.5595	496.3910	696.3930	0.198
		16	39.1638	81.1392	135.4962	157.3557	247.6979	353.8754	481.9316	628.7332	0.194
		32	39.1557	81.1198	135.4889	157.2887	247.5128	353.3915	480.8059	626.3504	0.194
		64	39.1552	81.1186	135.4884	157.2844	247.5008	353.3601	480.7322	626.1926	0.193
	20	4	45.3384	95.2442	208.2030	249.0036	319.4001	462.2149	677.8777	814.7213	0.116
		8	39.6672	84.6083	159.8522	233.2874	283.9409	364.1325	502.6177	708.1401	0.106
		16	39.2027	83.6075	157.6902	230.3056	282.3528	355.2960	485.9733	632.9262	0.099
		32	39.1725	83.5403	157.5390	230.0908	282.2329	354.6356	484.6245	630.2396	0.099
		64	39.1706	83.5359	157.5292	230.0766	282.2249	354.5917	484.5339	630.0581	0.099
	5	4	60.4554	62.0655	125.537	231.7259	378.9604	600.1897	627.8086	1253.0700	0.193
		8	60.0991	61.1552	123.4697	198.3449	297.4867	415.7805	549.9388	626.5810	0.187
		16	60.0726	61.0697	123.1223	197.0277	293.7024	407.1307	539.4764	625.9557	0.187
		32	60.0700	61.0602	123.0871	196.8993	293.3501	406.2818	537.6596	625.8876	0.187
		64	60.0693	61.0577	123.0789	196.8714	293.2851	406.1442	537.3988	625.8759	0.185
CC	10	4	63.4402	99.3857	146.5892	239.4079	390.4693	620.8316	1252.9286	2506.1168	0.188
		8	61.4983	96.7174	146.1027	200.5545	303.5004	423.9393	563.2567	793.0382	0.176
		16	61.2972	96.4318	145.7456	198.9650	299.3970	414.7870	552.7567	708.9513	0.175
		32	61.2824	96.4087	145.7206	198.8417	299.0730	413.9928	551.0206	705.4647	0.175
		64	61.2810	96.4056	145.7189	198.8287	299.0416	413.9194	550.8689	705.1703	0.173
	20	4	67.4057	115.3324	252.6964	259.9243	412.8944	637.9067	2505.6708	5012.2220	0.182
		8	62.0714	109.7196	202.3662	243.4657	321.4697	427.6925	569.0829	805.5803	0.122
		16	61.3885	108.5137	199.5638	241.7801	316.8809	416.9706	558.4235	714.8257	0.119
		32	61.3406	108.4228	199.3442	241.6479	316.5111	416.0037	556.4846	711.0692	0.119
		64	61.3374	108.4163	199.3285	241.6379	316.4855	415.9340	556.3459	710.7998	0.118

Table.2: Comparison of dynamic buckling loads against geometric parameter ($\boldsymbol{\lambda}$) for HH classical for the present study with analytical solutions [7].

$\boldsymbol{\lambda}$	**Dynamic Buckling Load (P_{cr})**	
	Present	**Ref. [7]**
5	0.213	0.198
7	0.199	0.203
9	0.195	0.194
10	0.194	0.196
13	0.170	0.155
15	0.126	0.134
17	0.112	0.115
19	0.110	0.099
20	0.099	0.093
23	0.090	0.077
25	0.086	0.070
27	0.083	0.0650
29	0.081	0.059
31	0.079	0.054
33	0.079	0.050
35	0.078	0.048

Table 3: Comparison of critical dynamic buckling load $\overline{P}_{cr}$ of *HH* classical graphene platelets reinforced composite curved beam under centrally applied point load P_p with Ref [16] ($\bar{P} = \frac{P_p}{N_{E0}\theta}$; $N_{E0} = \frac{(1.4303\pi)^2 Ebh^3}{3L^2}$, $\frac{L}{h} = 50, \lambda = 10, W_{gpl} = 0.1\%$).

Multilayer Arch	$\boldsymbol{W_{gpl}}$	**Present**	**Ref. [16]**
U-GPLRC	0.1%	0.3729	0.3812
	0.3%	0.5616	0.5744
	0.5%	0.7508	0.7676
Pure Epoxy	0.0%	0.2785	0.2846

Table 4: Comparison of non-dimensional natural frequencies of HH non-classical curved beam ($\phi = 60°$) for different nonlocal parameter ($\boldsymbol{\mu}$) against analytical solutions [46]. ($\bar{\omega}_i = \omega L^2\sqrt{\frac{m}{EI}}$)

L/h	$\boldsymbol{\mu}$	**SIN Model (Present)**			**Sol 1 [46]**		
		$\overline{\omega_1}$	$\overline{\omega_2}$	$\overline{\omega_3}$	$\overline{\omega_1}$	$\overline{\omega_2}$	$\overline{\omega_3}$
10	0	8.1837	35.5630	76.7076	8.1991	35.7451	77.3993
	1	7.8075	30.1123	55.8222	7.8222	30.2666	56.3256
	2	7.4788	26.5842	46.0349	7.4929	26.7204	46.4500
	3	7.1884	24.0623	40.0695	7.2020	24.1855	40.4308
	4	6.9294	22.1442	35.9490	6.9425	22.2576	36.2732
50	0	8.3171	37.7569	86.6665	8.3177	37.7658	86.7084
	1	7.9347	31.9701	63.0696	7.9353	31.9776	63.1000
	2	7.6007	28.2243	52.0116	7.6013	28.2309	52.0367
	3	7.3055	25.5467	45.2717	7.3061	25.5527	45.2935
	4	7.0423	23.5104	40.6162	7.0429	23.5159	40.6359

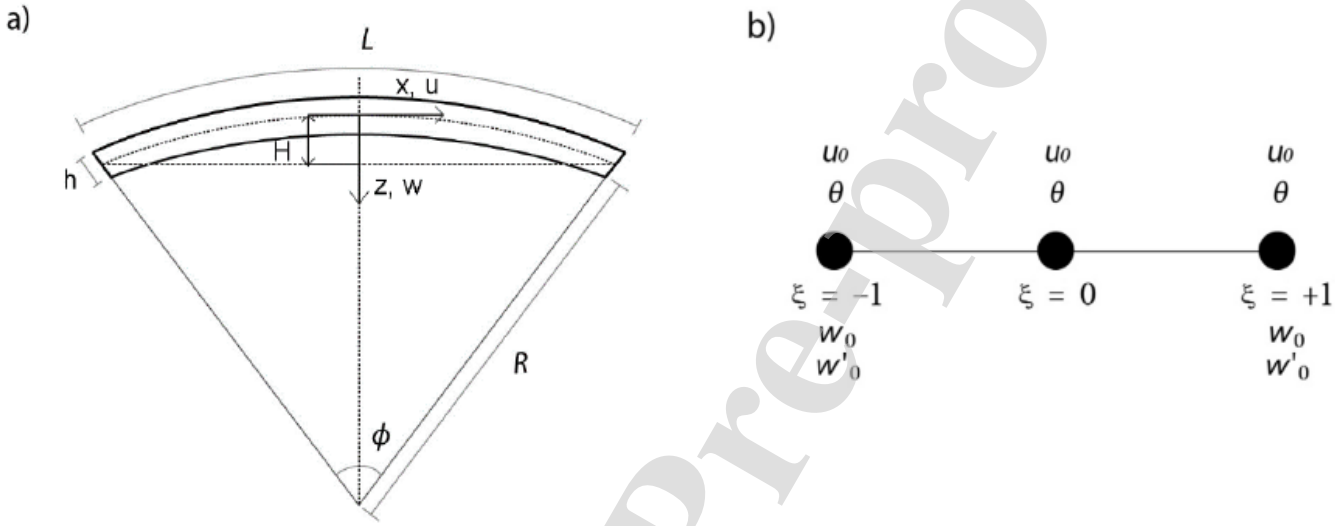

Fig.1: a) Geometrical parameters of curved beam b) Beam element with the degrees of freedom.

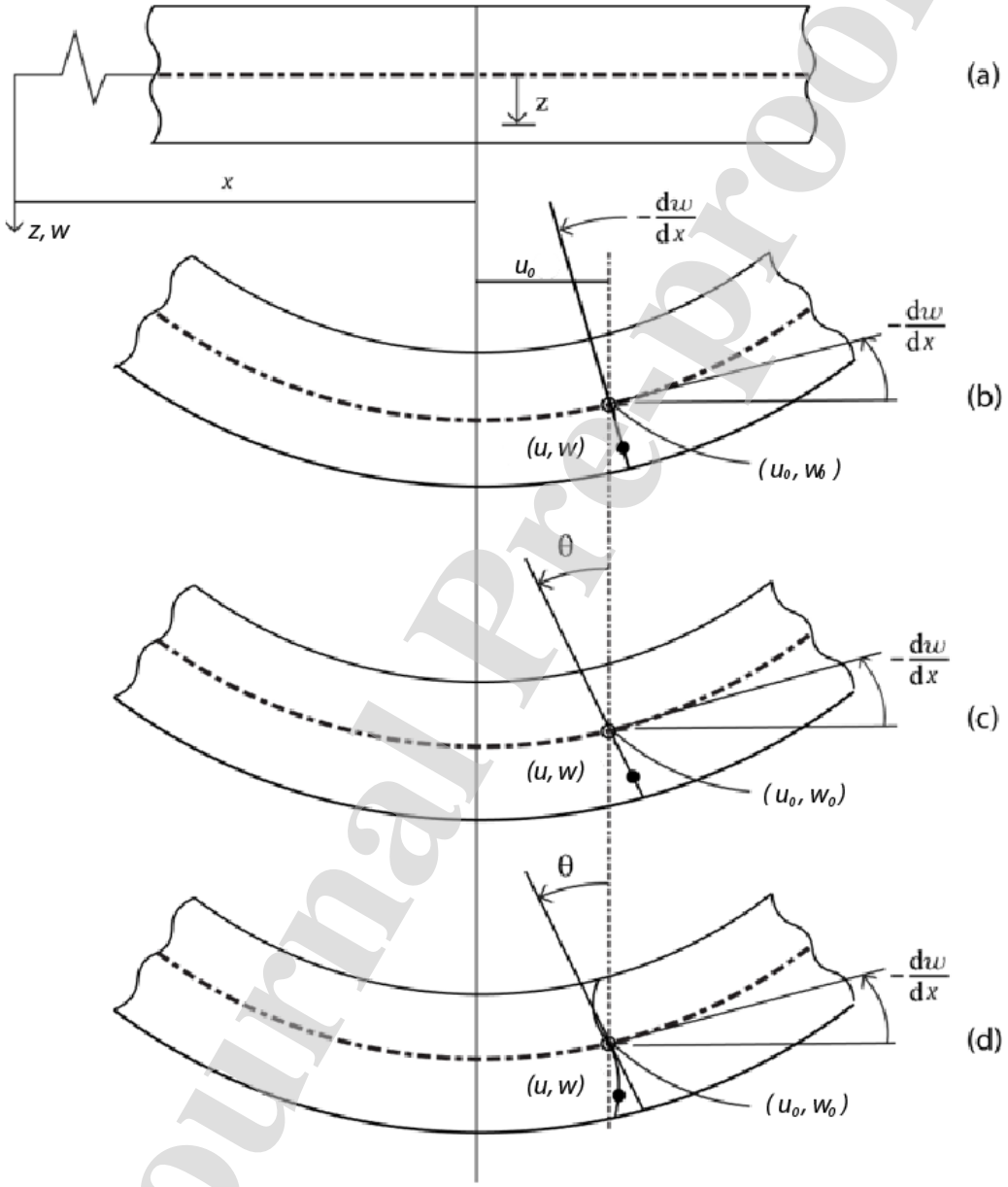

Fig. 2. Un-deformed and deformed geometry of a beam section: (a) un-deformed; (b) Euler-Bernoulli; (c) Timoshenko; (d) higher order theories

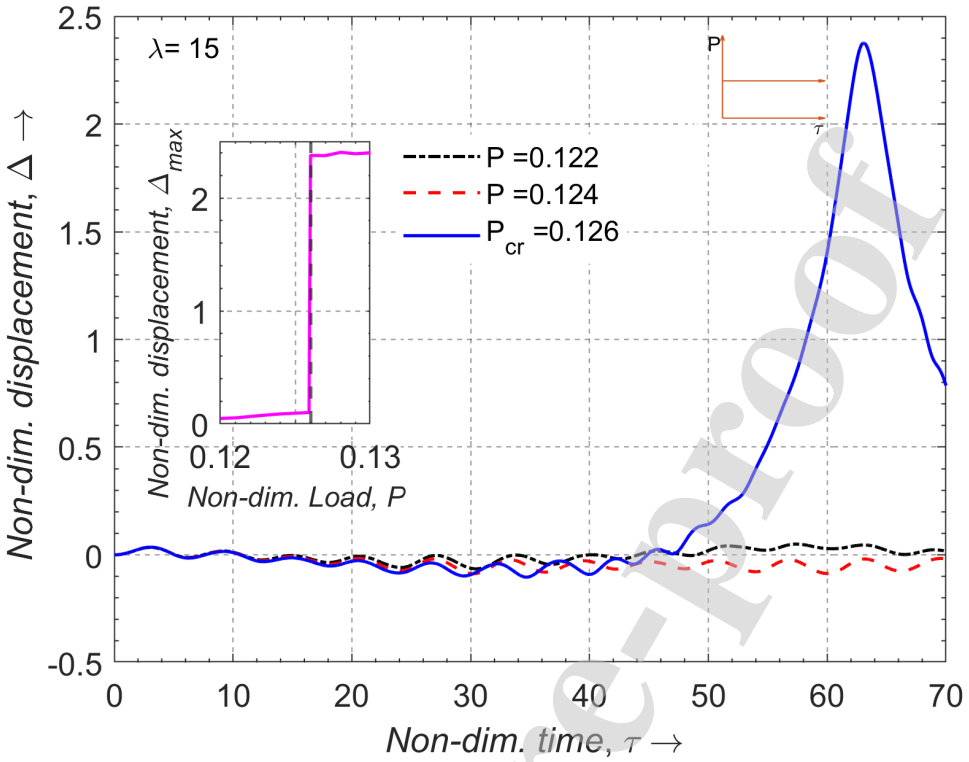

Fig. 3a: The load versus time response of classical HH curved Beam for $\lambda = 15$.

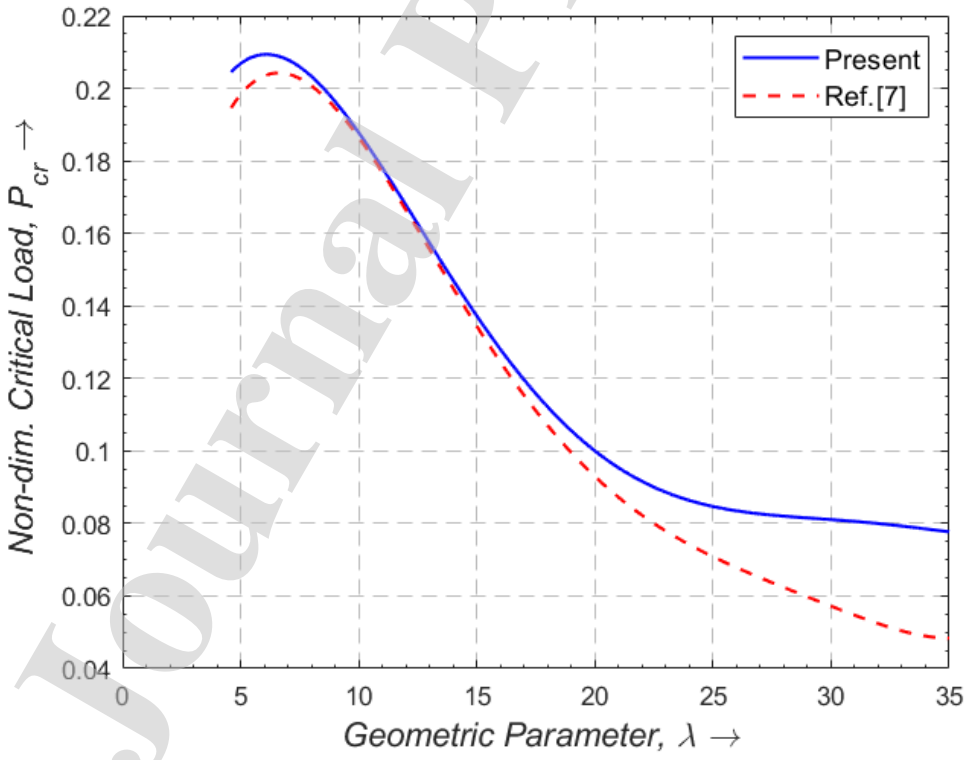

Fig. 3b: Variation of dynamic critical load against geometric parameter ($\boldsymbol{\lambda}$) for HH classical curved beam along with Ref. [7].

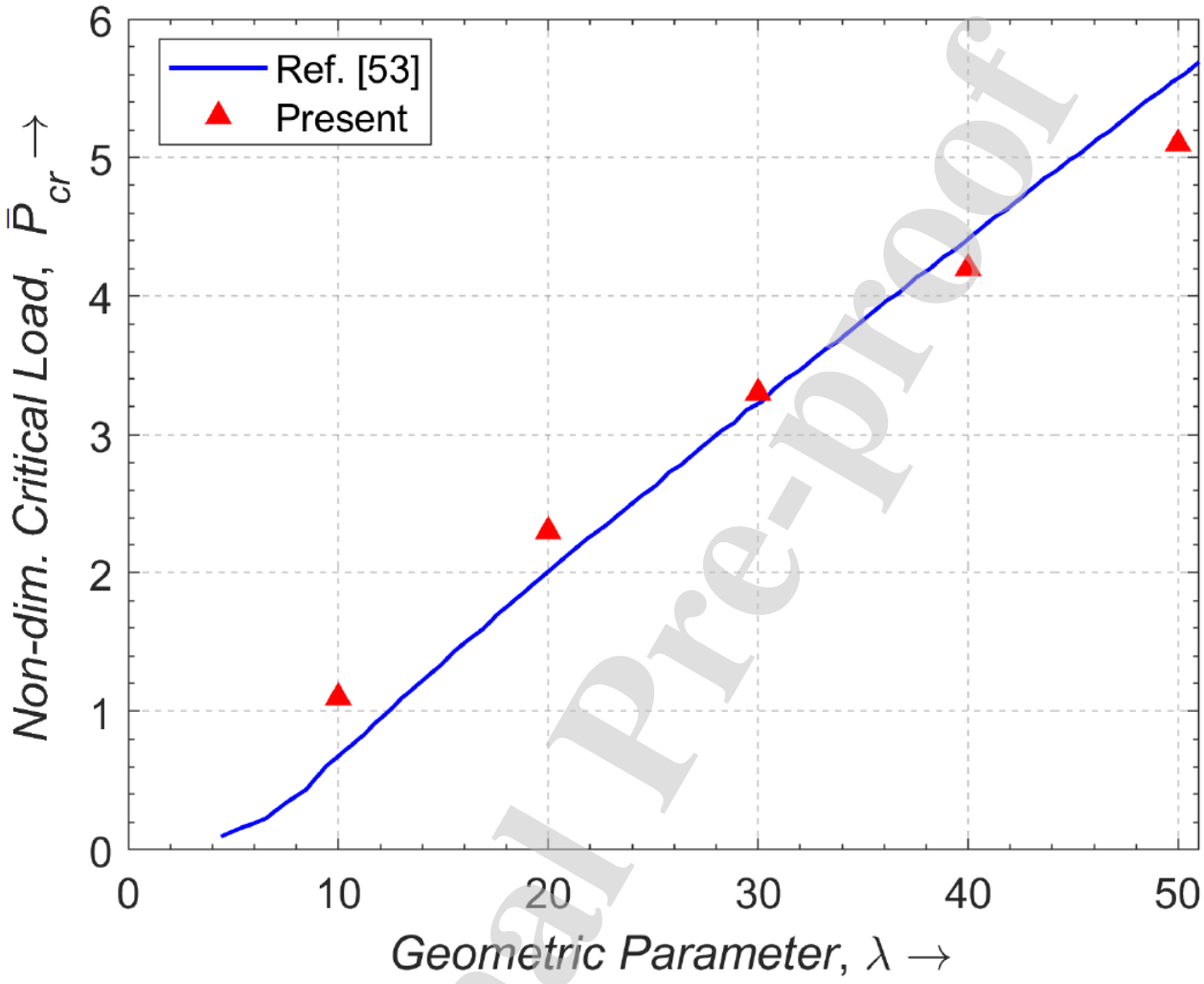

Fig. 4: Variation of dynamic critical load $\bar{P}_{cr}$ with geometric parameter λ for HH classical isotropic curved beam under centrally applied point load P_p along with Ref. [53] ($\bar{P}_{cr} = \frac{P_p L^2}{8EI}$).

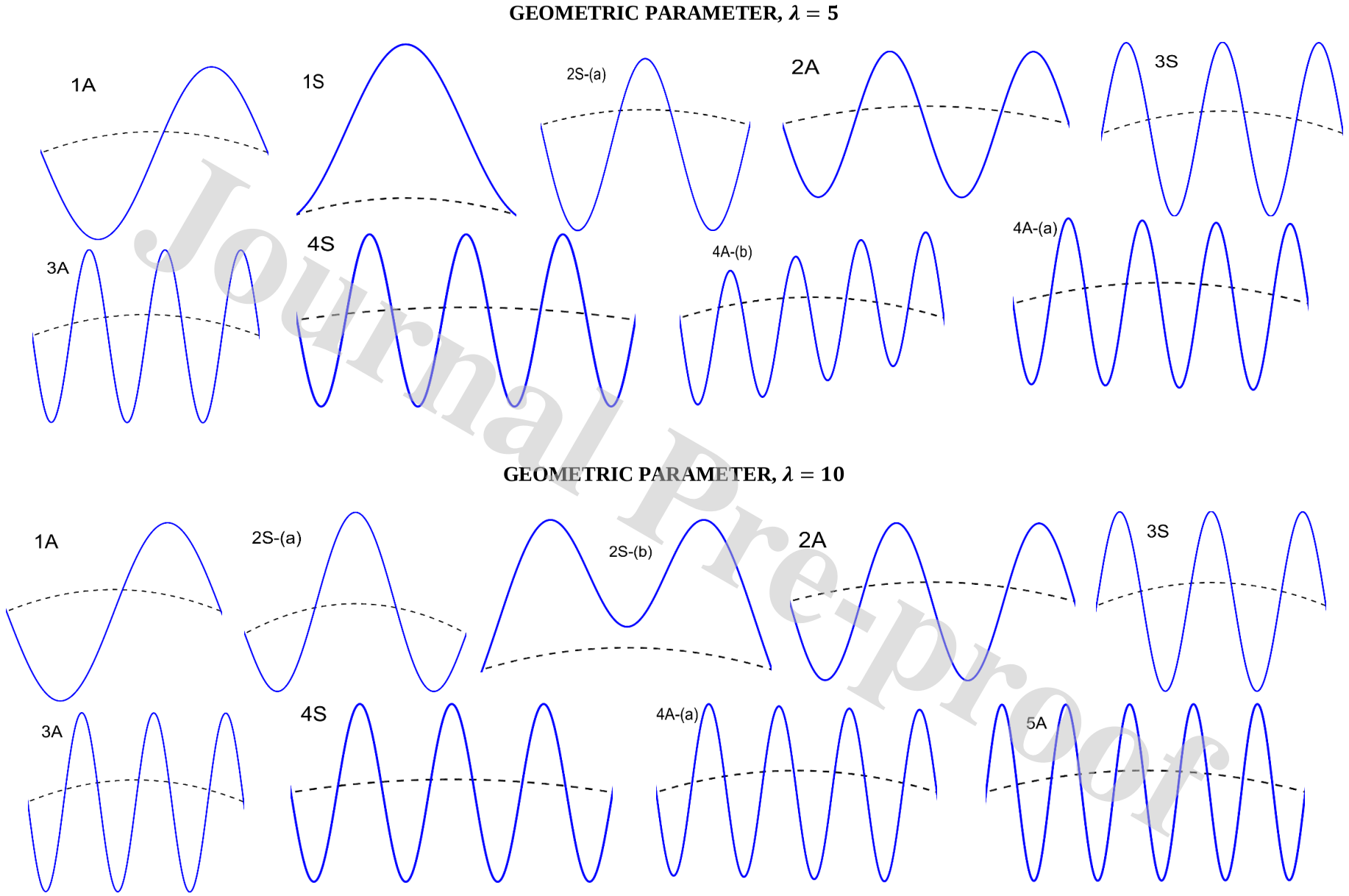

Fig.5: Representation of different types of natural free vibration mode shapes of HH classical curved beam with geometric parameter, $\lambda = 5$ &10.

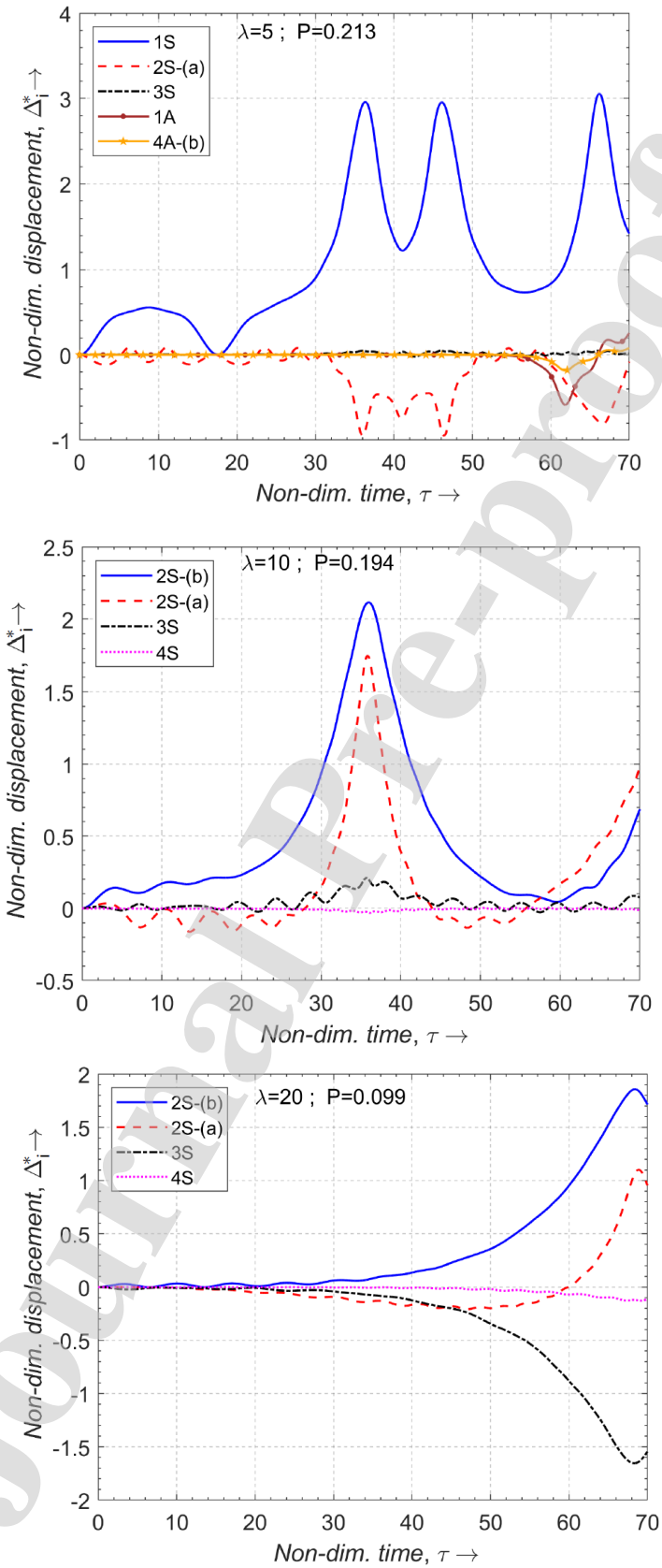

Fig.6: Modal participation factors for HH classical curved beam with $\boldsymbol{\lambda}$ =5, 10 & 20, and at certain loads, P.

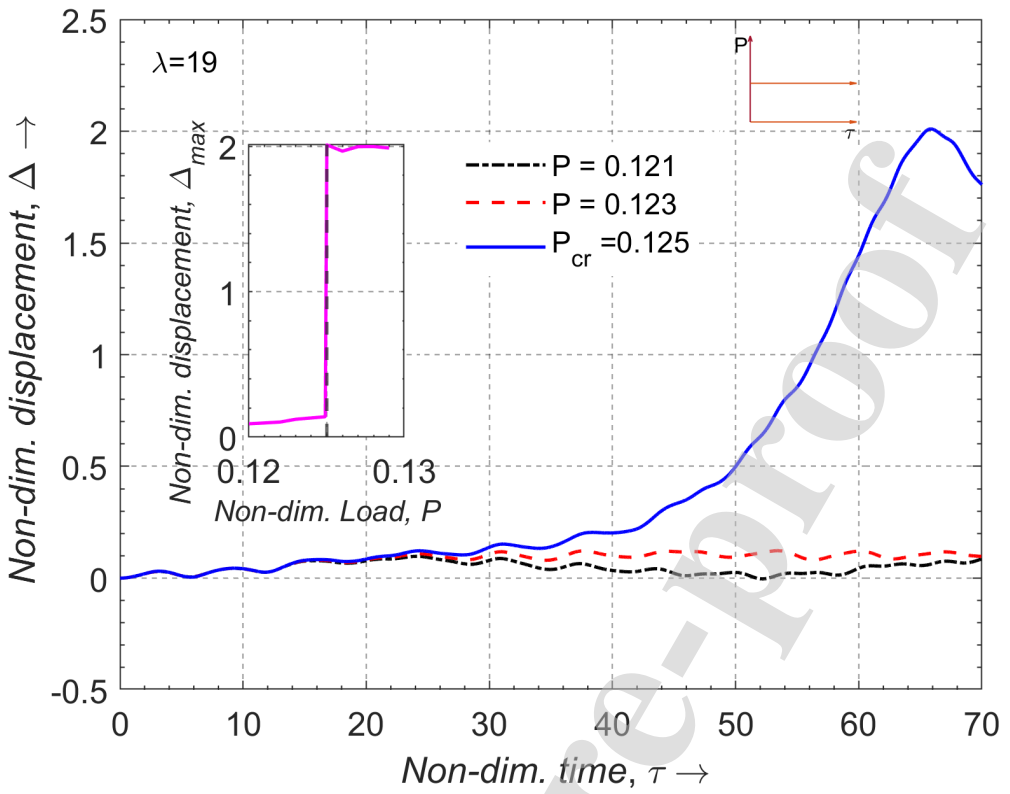

Fig.7a: The load versus time response of CC classical curved Beam for $\lambda = 19$.

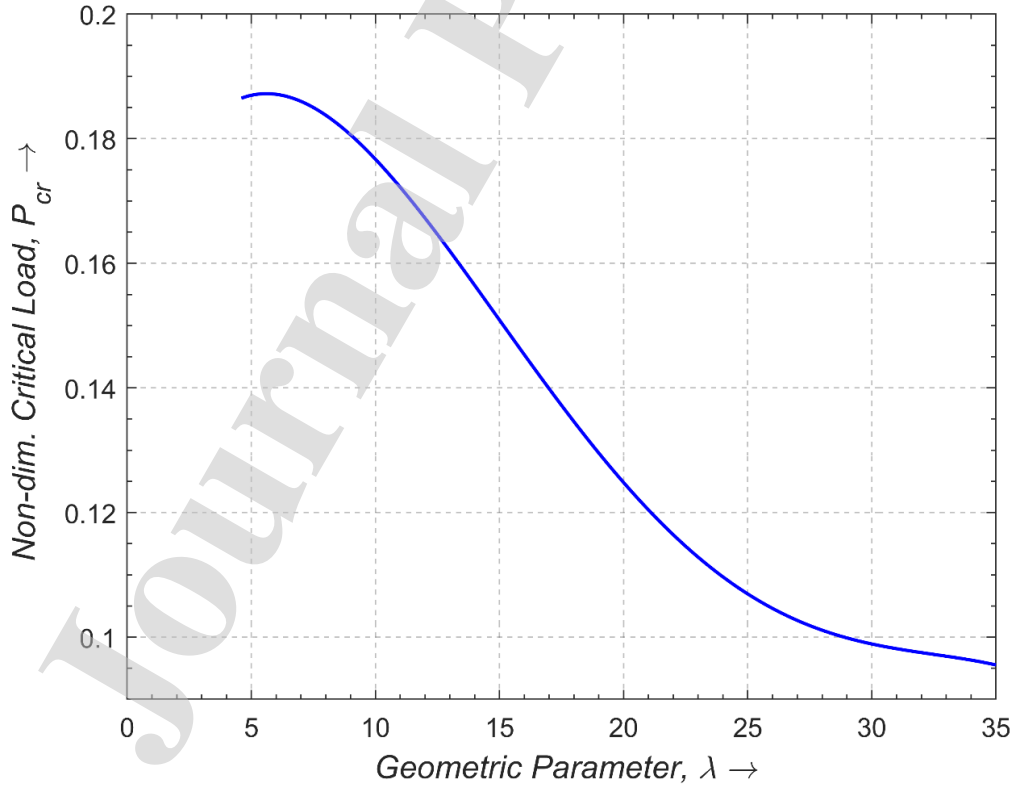

Figure 7b: Variation of dynamic critical load against geometric parameter ($\boldsymbol{\lambda}$) for CC classical curved beams.

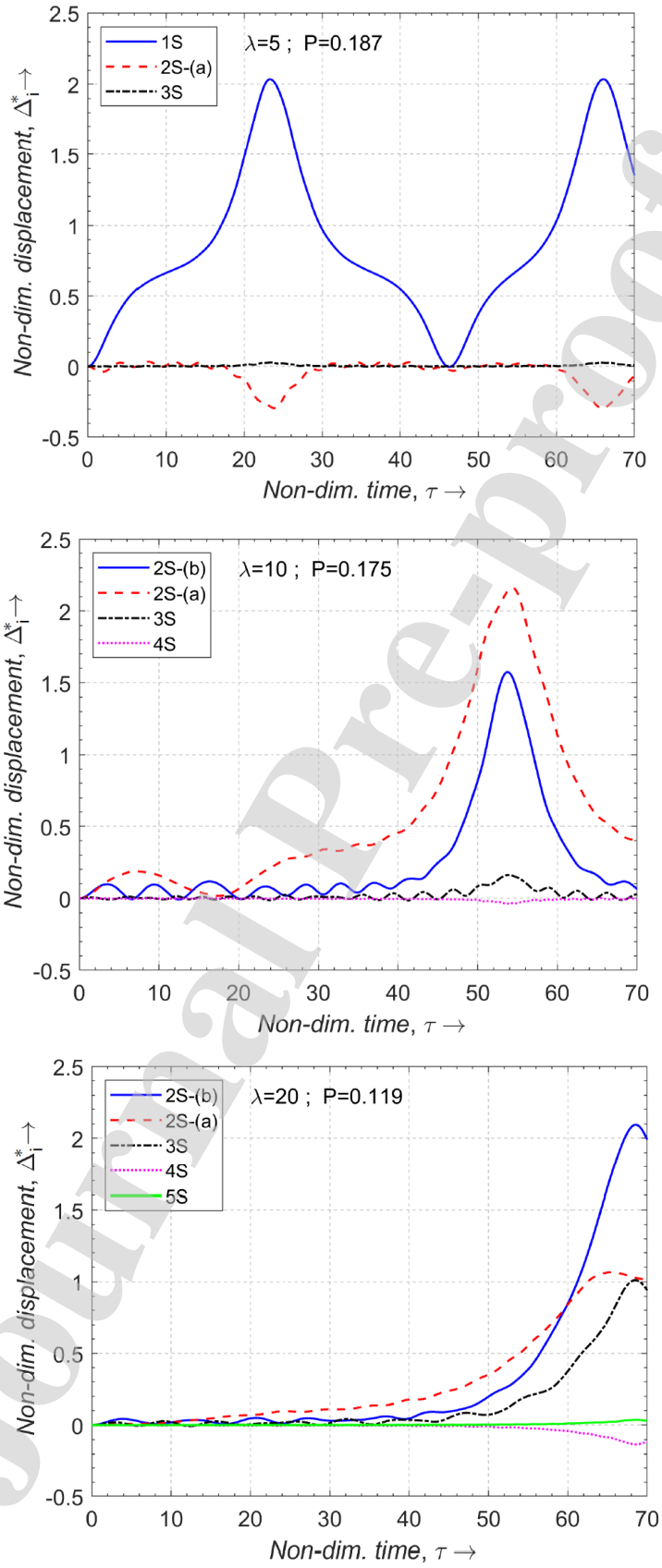

Fig.8: Modal participation factors for CC classical curved beam with $\boldsymbol{\lambda}$ =5, 10 & 20, and at certain loads, P.

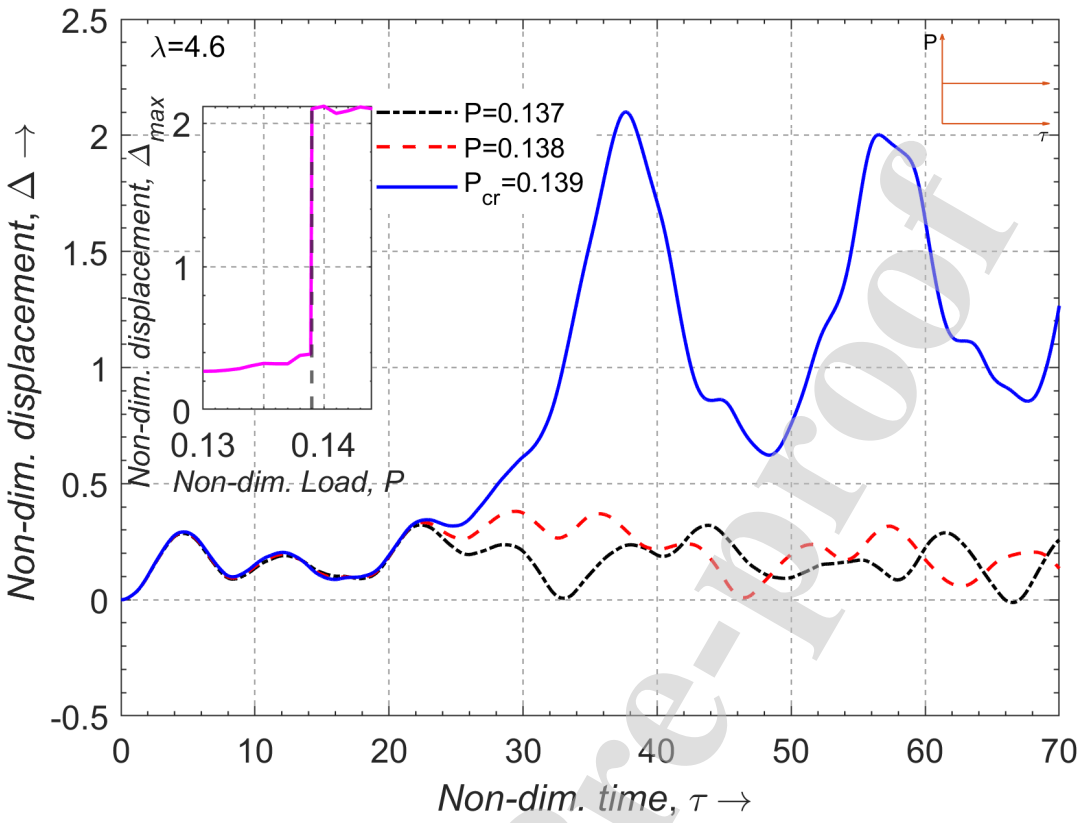

Fig.9a: The load versus time response of CH classical curved Beam for $\lambda = 4.6$.

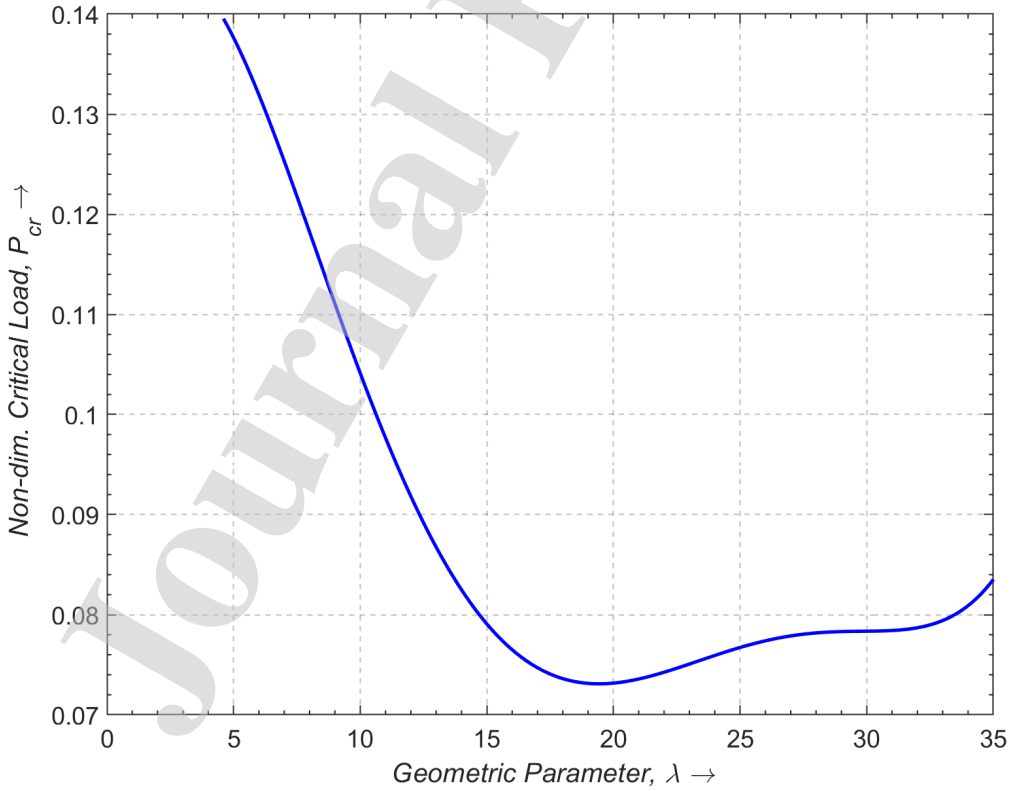

Fig. 9b: Variation of dynamic critical load against geometric parameter ($\boldsymbol{\lambda}$) for CH classical curved beams.

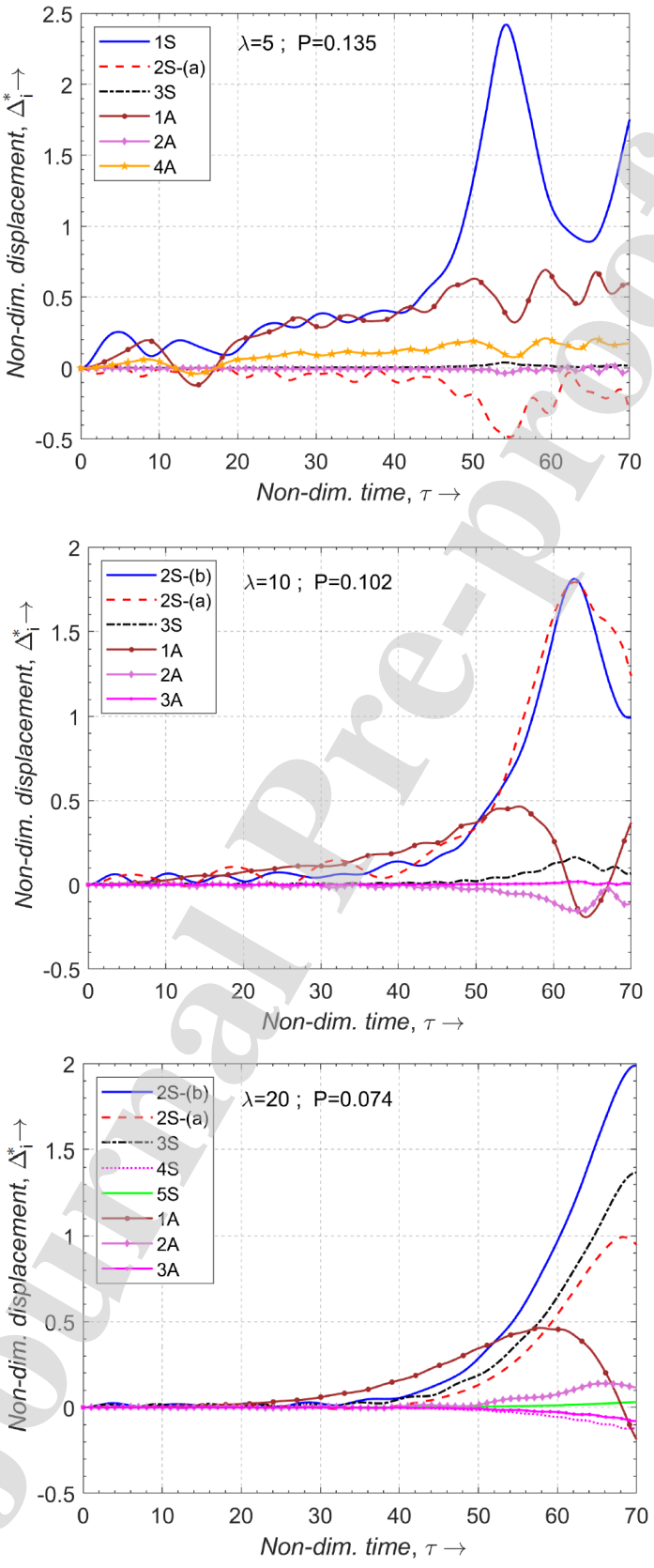

Fig.10: Modal participation factors for CH classical curved beam with $\boldsymbol{\lambda}$ =5, 10 & 20, and at certain loads, P.

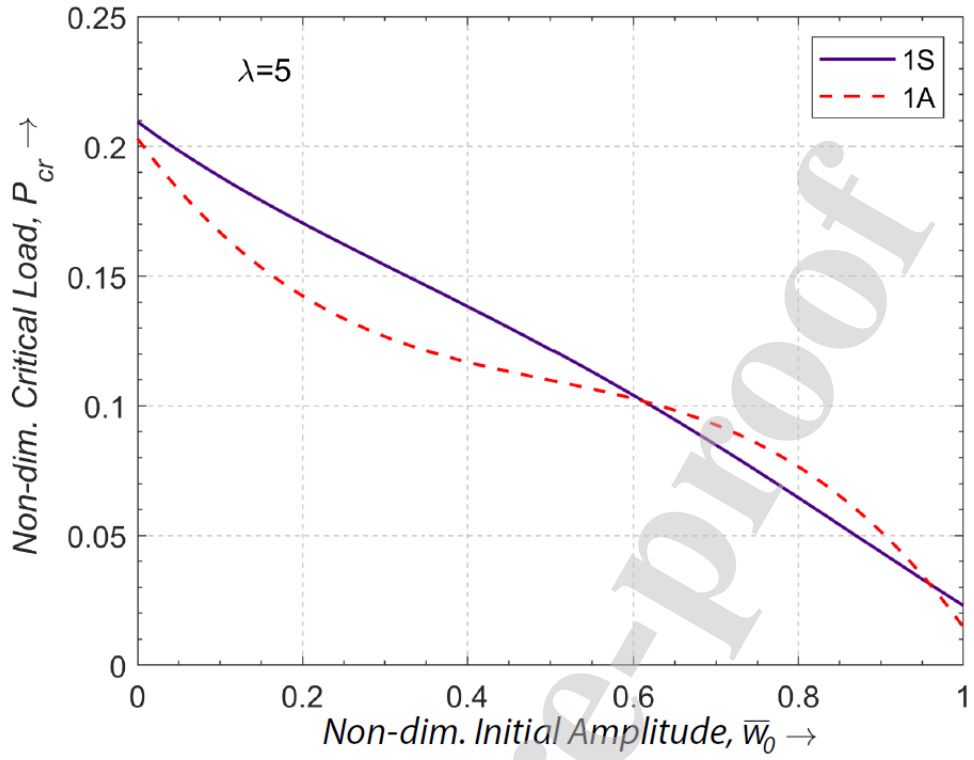

(a)

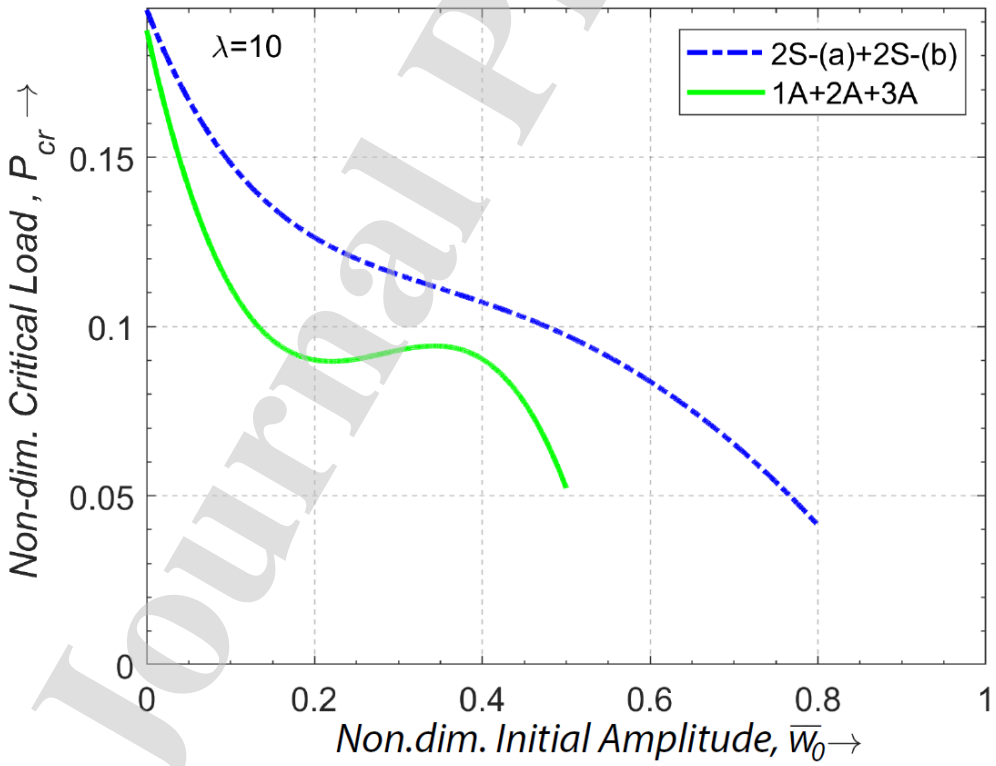

(b)

Fig. 11: Variation of dynamic critical load against initial amplitude, ($\overline{w}_0$) for HH classical curved beam with $\boldsymbol{\lambda}$ =5 & 10 (a) single mode perturbation; (b) multi-modes perturbation.

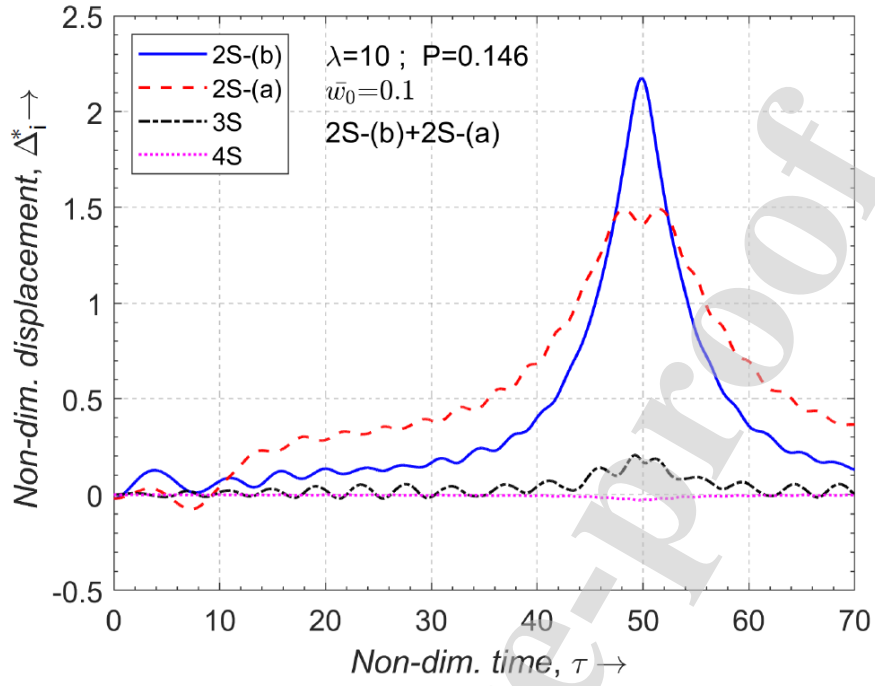

(a)

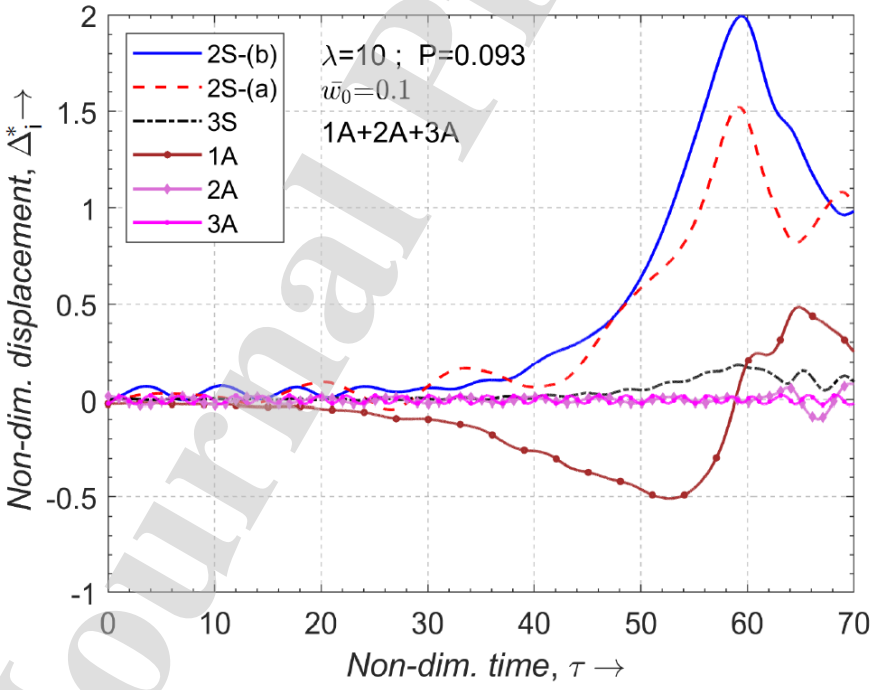

(b)

Fig. 12: Modal participation factors for HH classical curved beam with $\boldsymbol{\lambda}$ =10, and initial amplitude ($\bar{w}_0 = \mathbf{0.1}$) at certain loads, P: (a) symmetric multi-modes perturbation; (b) asymmetric multi-modes perturbation.

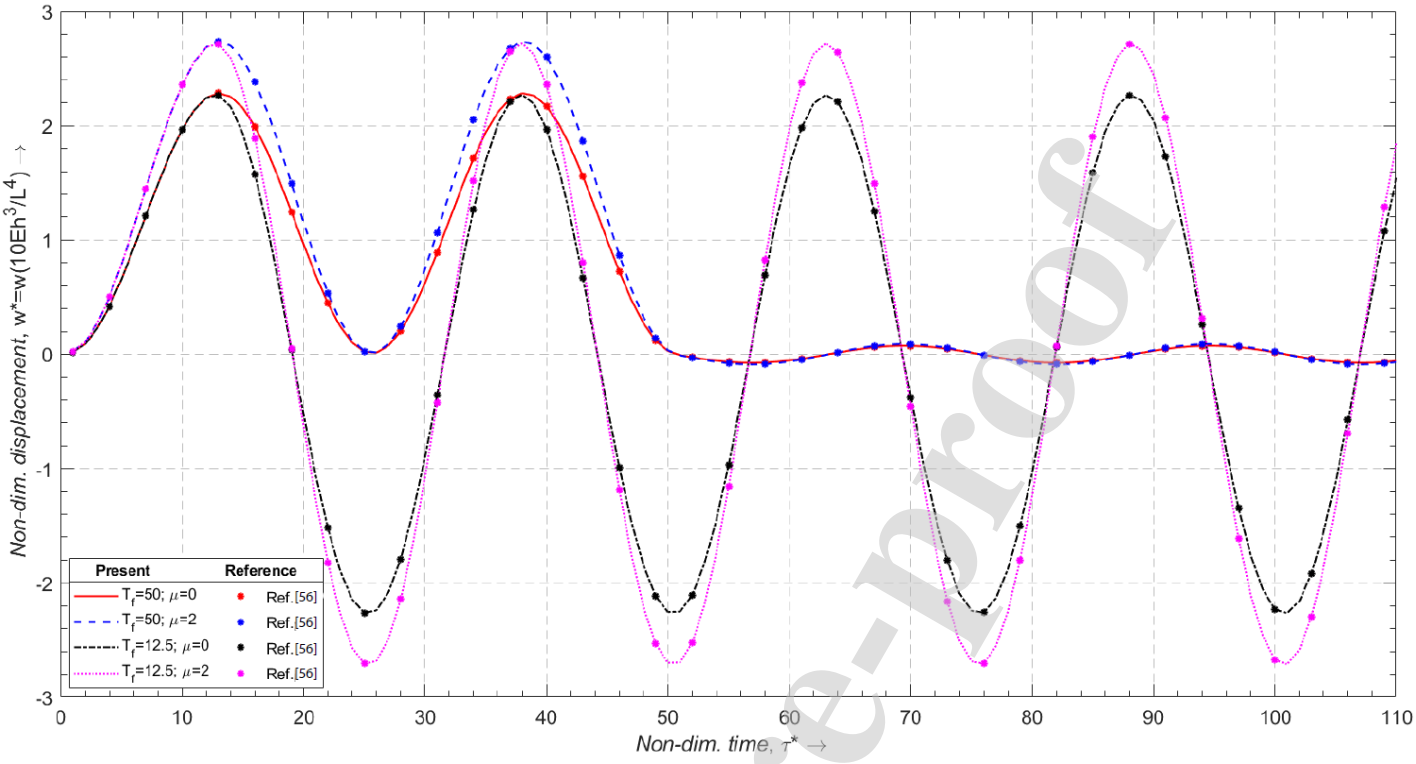

(a)

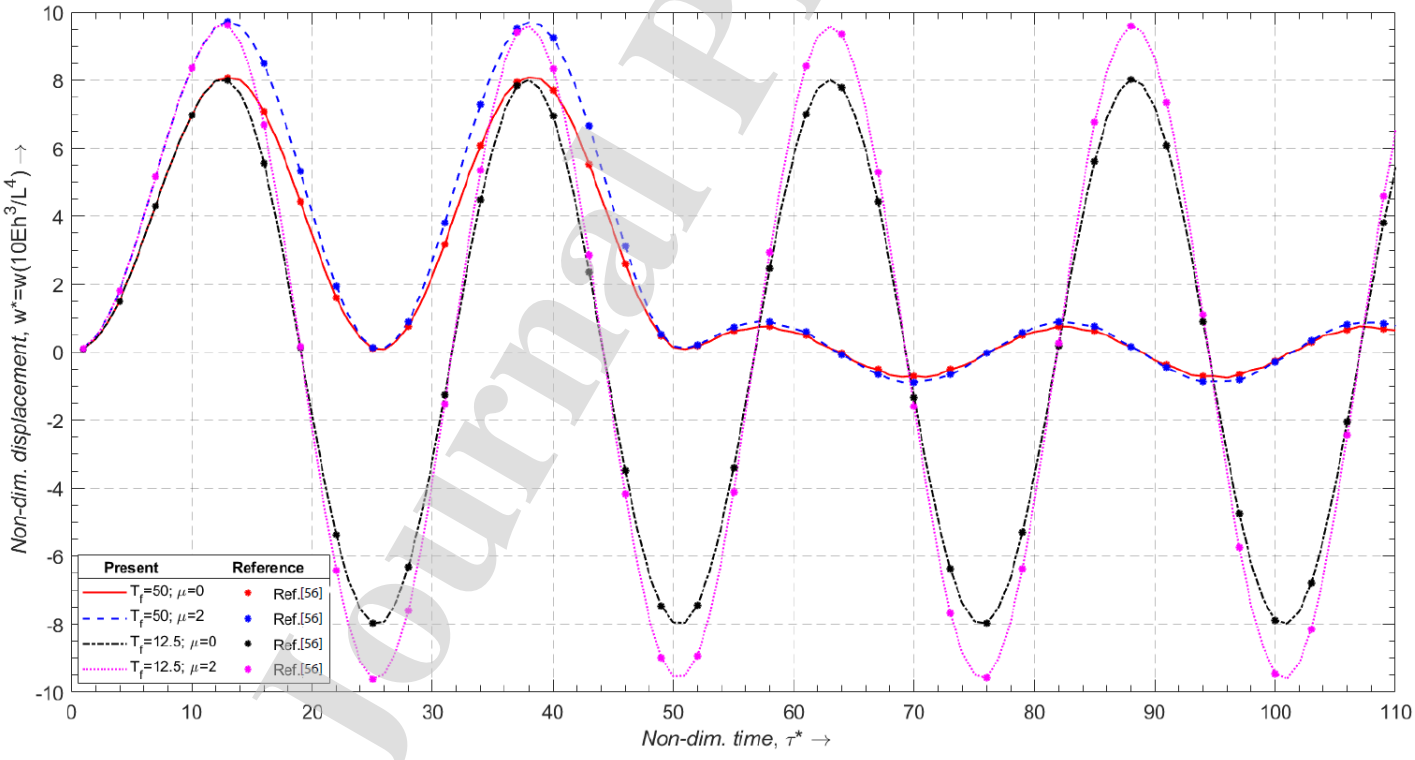

(b)

Fig. 13: Comparison of linear transient response of HH non-classical thick curved beam (L/h=5) with analytical solutions [47]: shallow nanobeam, (a) $\theta = 15°$; (b) deep nanobeam, $\theta = 120°$.

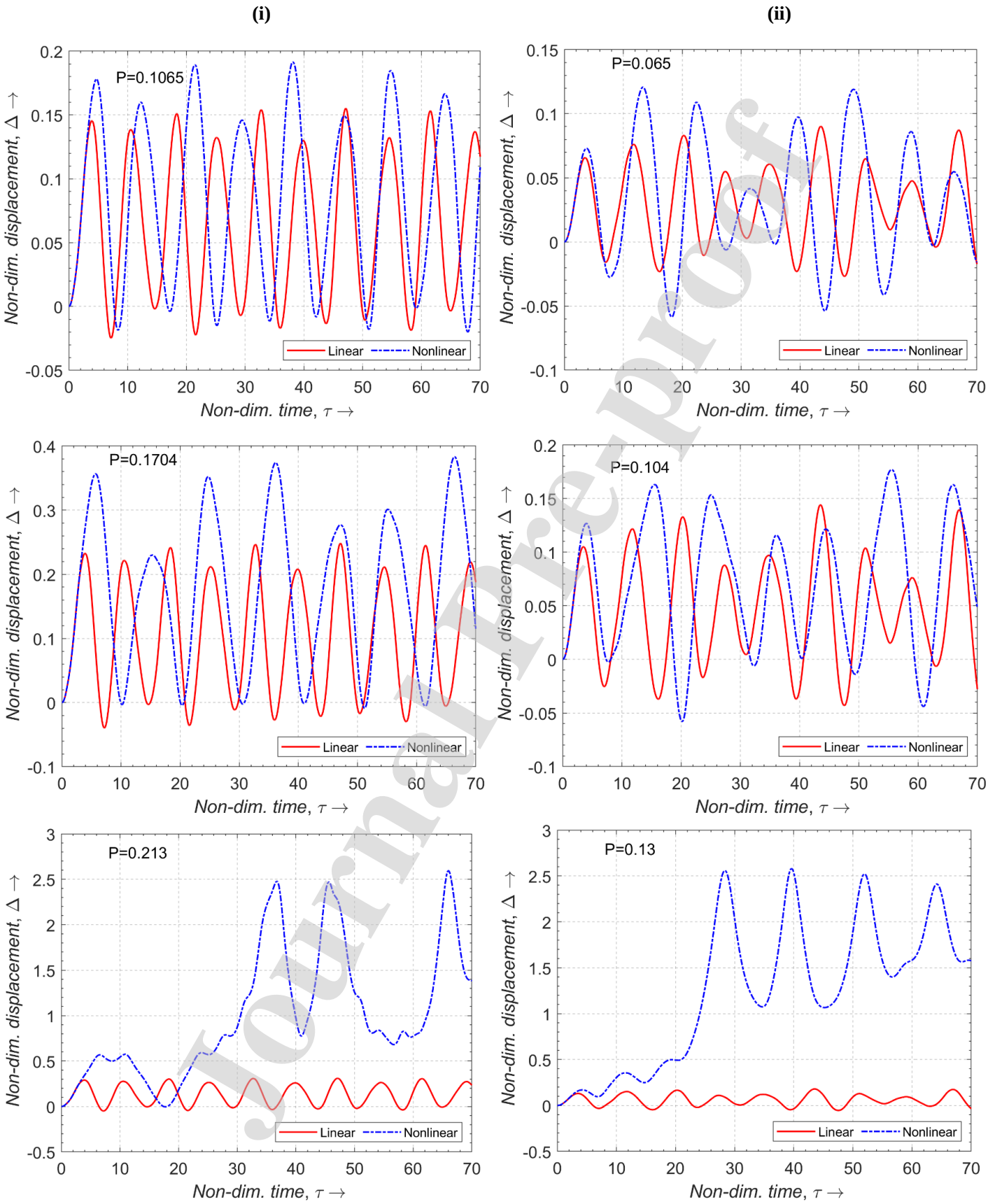

Fig. 14: Linear and nonlinear transient response of HH non-classical curved beam (λ =5) with two local parameter: (i) $\mu = 0$; (i) $\mu = 4$

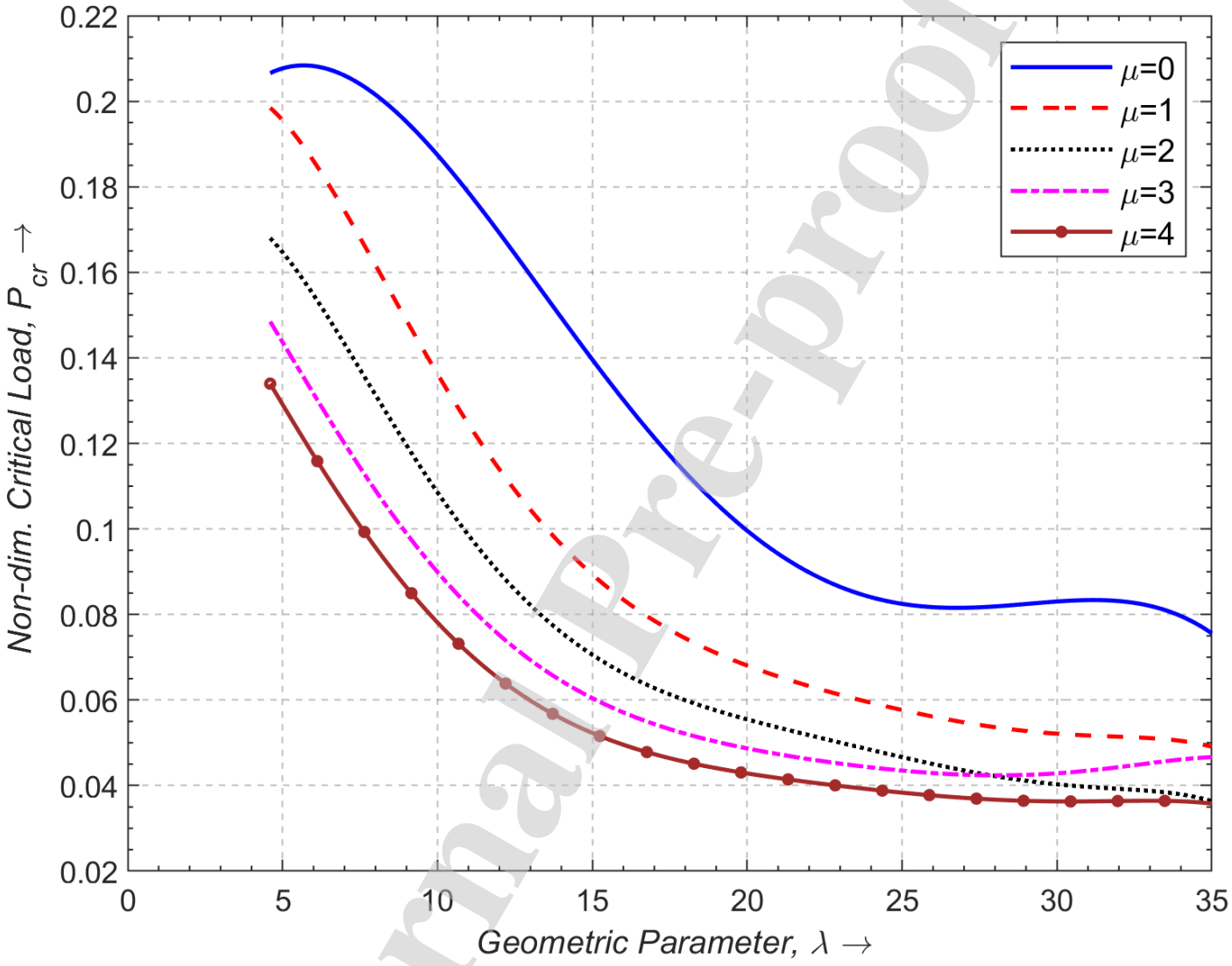

Fig.15: Variation of dynamic critical load against geometric parameter ($\boldsymbol{\lambda}$) for HH non-classical curved beams with different nonlocal parameter (μ)

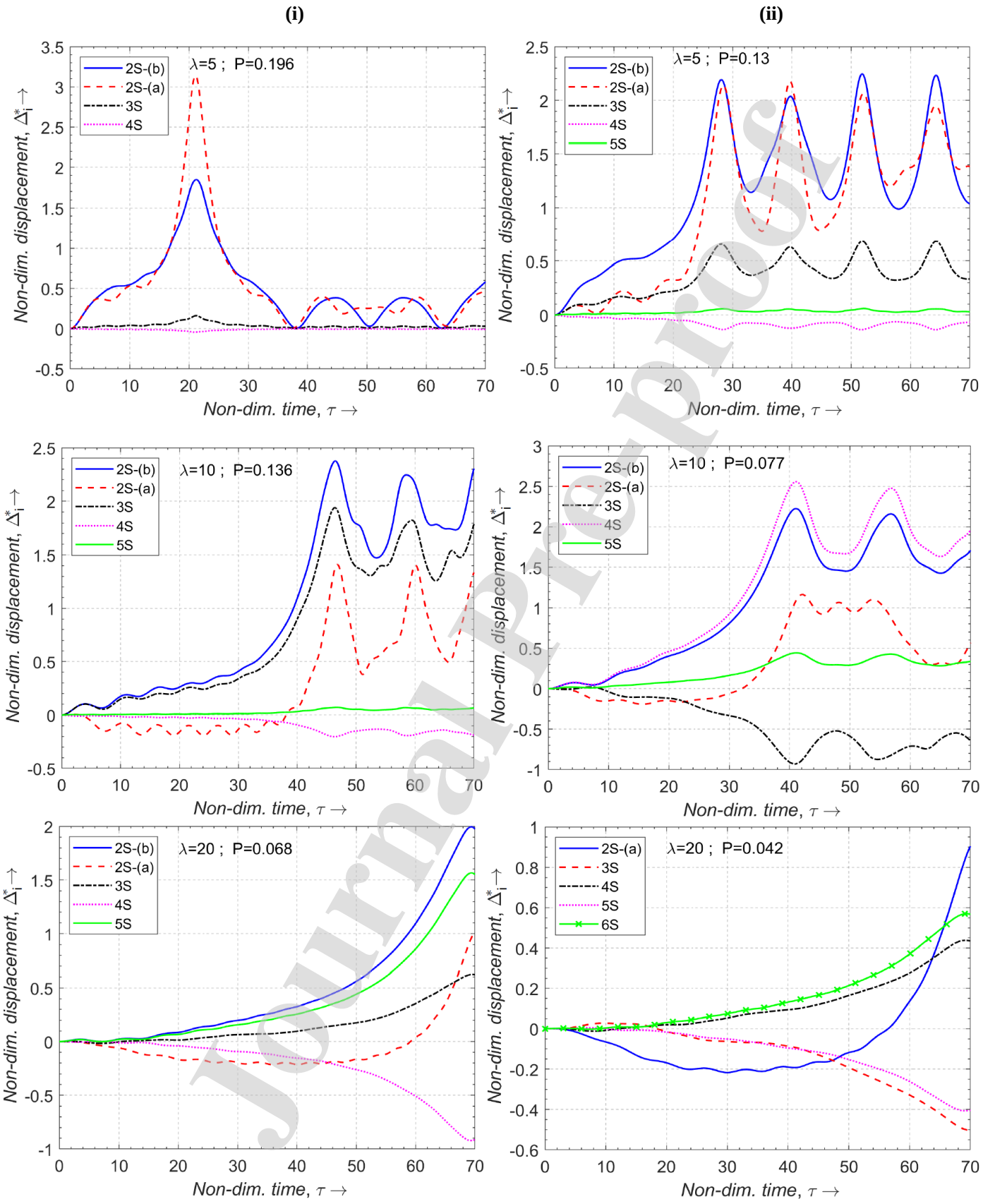

Fig. 16: Modal participation factors for HH non-classical curved beam with $\boldsymbol{\lambda}$ =5, 10 & 20, and at certain load, P:(i) μ=1; (ii) μ=4

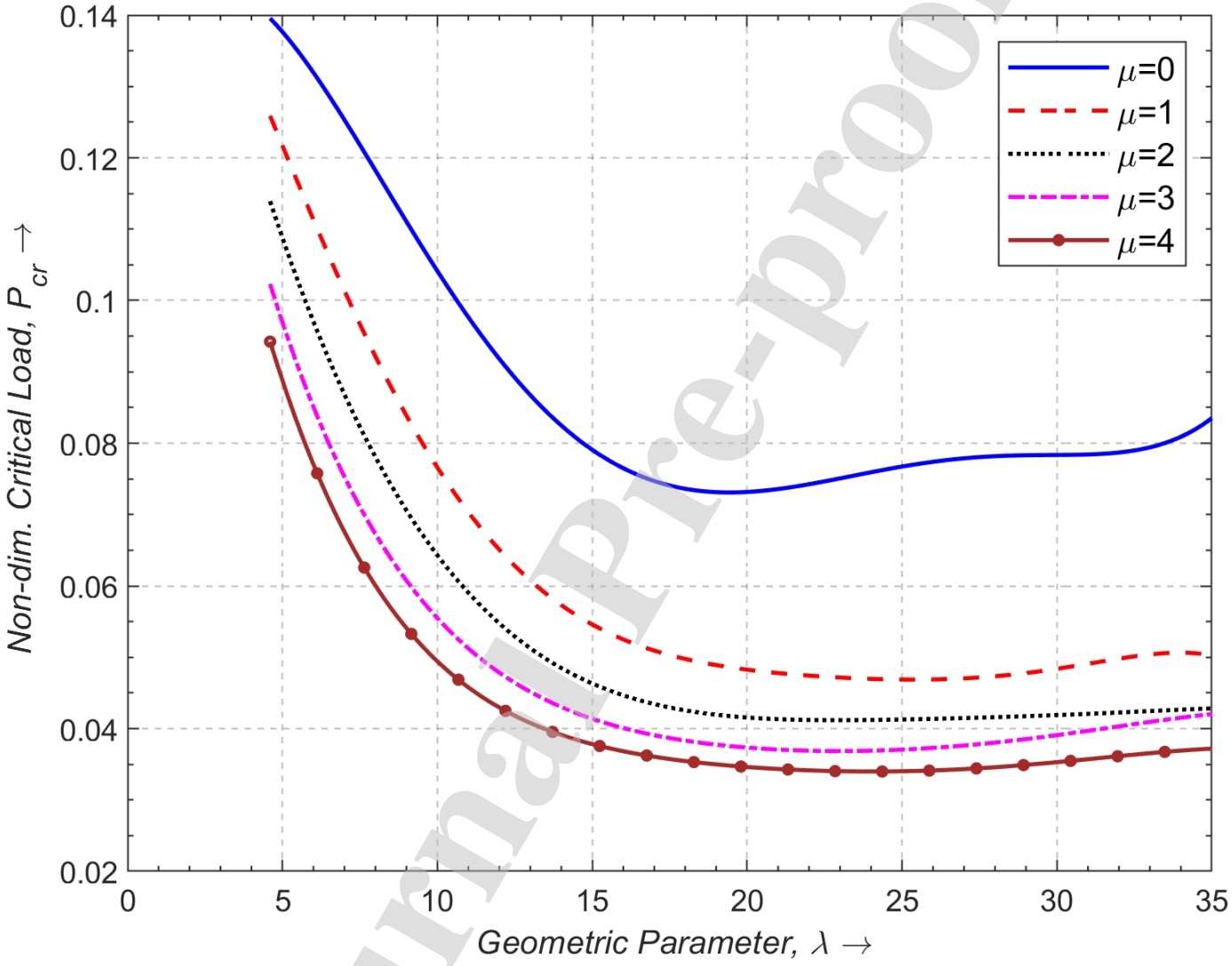

Fig.17: Variation of dynamic critical load against geometric parameter ($\boldsymbol{\lambda}$) for CH non-classical curved beams with different nonlocal parameter (μ)

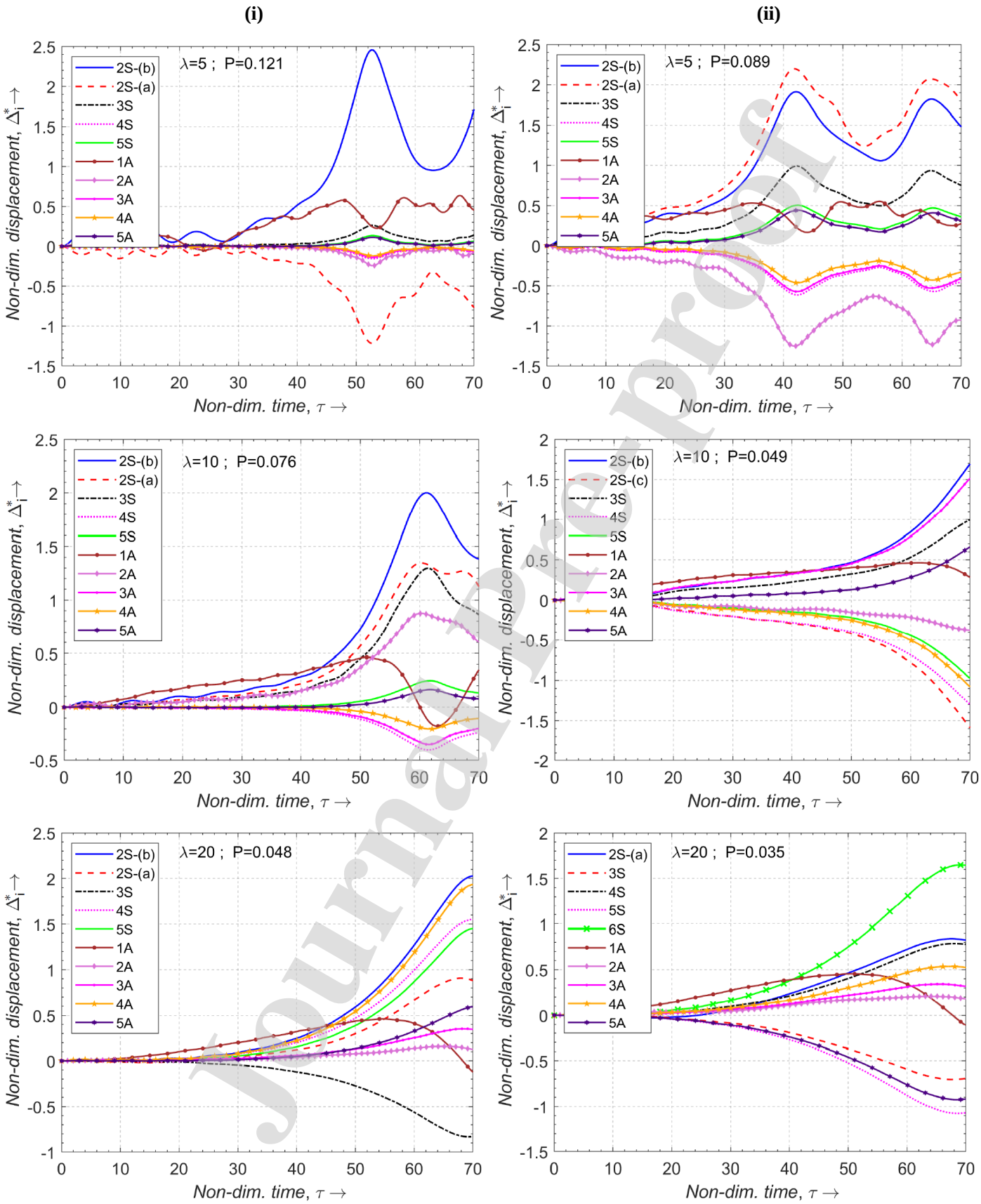

Fig.18: Modal participation factors for CH non-classical curved beam with $\boldsymbol{\lambda}$ =5, 10 & 20, and at certain load, P:(i) μ=1; (ii) $\mu = 4$

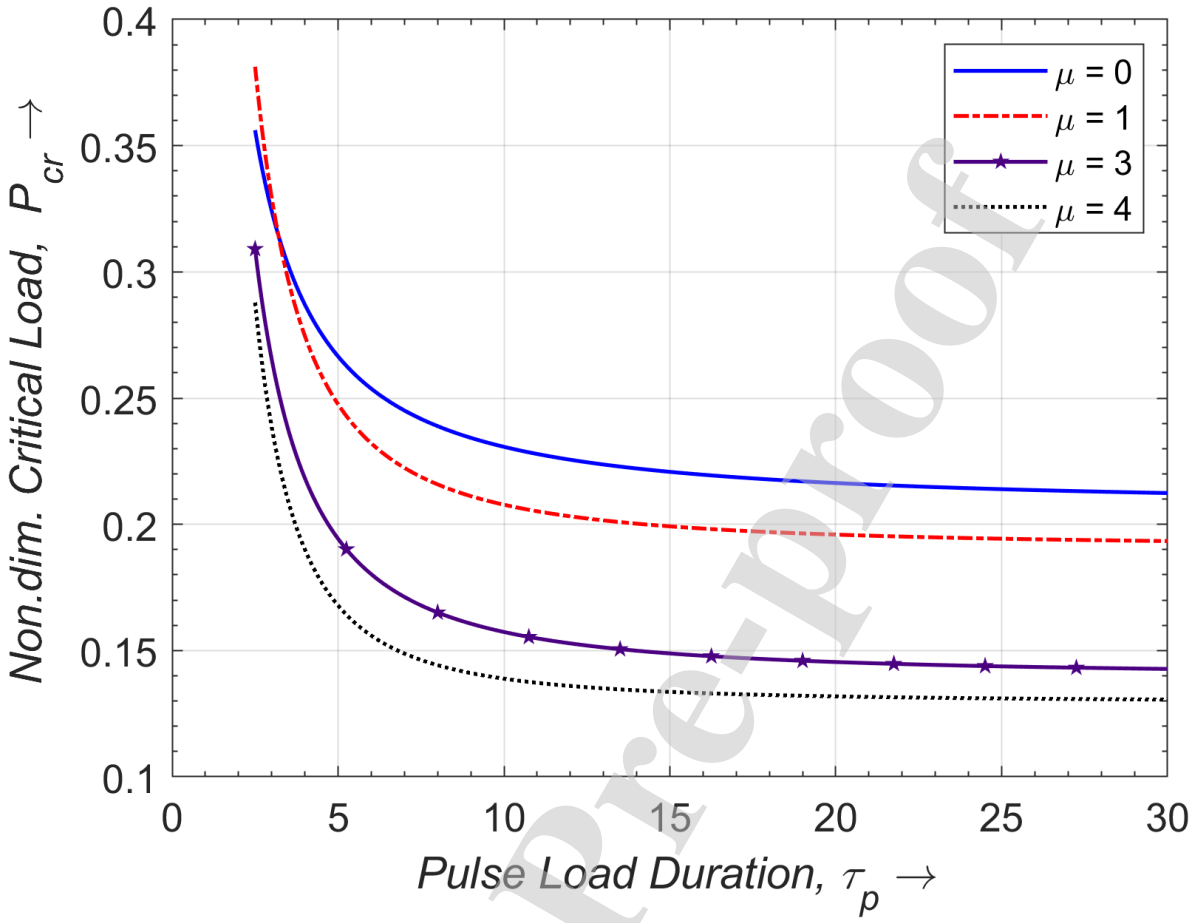

(a)

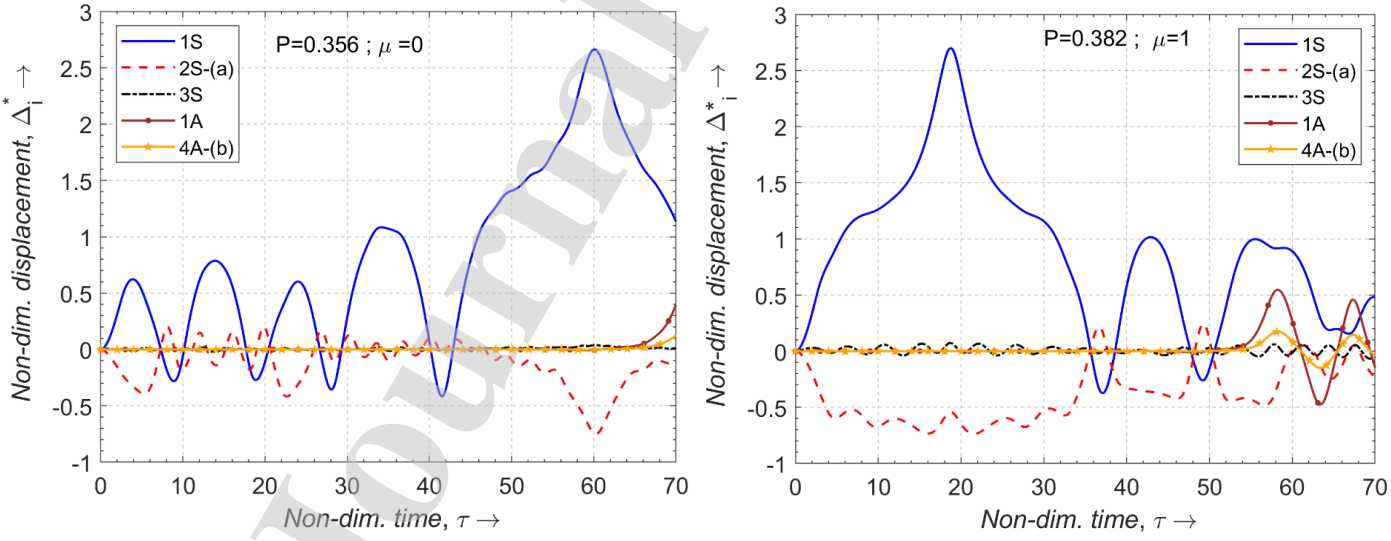

(b)

Fig. 19: Variation of dynamic critical load and modal responses for HH non-classical curved beams $\boldsymbol{\lambda}$ =5 with finite pulse load duration (τ_p): (a) P_{cr} versus τ_p; (b) Modal response for pulse load duration τ_p = 2.5 (μ=0 & 1).

Highlights

- Derived nonlocal nonlinear dynamic governing equations for finite element model for curved nanobeam in terms of generalized displacements.
- Formulation includes size dependent effect for non-classical curved beam by nonlocal elasticity theory.
- Finite element based on higher-order shear deformation theory and solutions by time response analysis.
- Established the dynamic critical load through load-deflection relation obtained from time responses.
- Evaluated the degree of participation of natural modes *a posteriori* by modal expansion approach.
- Study on highlight the limitation of assumed-modes in nonlinear analytical formulation.
- Presented benchmark results for assessing other theories and solution approaches.

Author statement:

Ganapathi Manickam & Olivier Polit: Conceptualization, Methodology, Validation, Final draft preparation. **Vasudevan Rajamohan:** Algorithm development, Investigation, Reviewing and Editing. **De Sarthak & Prateek Gupa:** Software, Validation, investigation, Initial draft preparation

Conflicting of interests declaration

The authors had no conflicts of interests in any form pertaining to this work.

Funding

The authors had no financial support in any form for carrying out this research work.